Modeling of the Piezoelectric-Driven Stick-Slip Actuators

A Thesis Submitted to the College of

Graduate Studies and Research

In Partial Fulfillment of the Requirements

For the Degree of Master of Science

In the Department of Mechanical Engineering

University of Saskatchewan

Saskatoon

By

Dong Kang

Permission to Use

In presenting this thesis in partial fulfilment of the requirements for a Postgraduate degree from the University of Saskatchewan, I agree that the Libraries of this University may make it freely available for inspection. I further agree that permission for copying of this thesis in any manner, in whole or in part, for scholarly purposes may be granted by the professor or professors who supervised my thesis work or, in their absence, by the Head of the Department or the Dean of the College in which my thesis work was done. It is understood that any copying or publication or use of this thesis or parts thereof for financial gain shall not be allowed without my written permission. It is also understood that due recognition shall be given to me and to the University of Saskatchewan in any scholarly use which may be made of any material in my thesis.

Requests for permission to copy or to make other use of material in this thesis in whole or part should be addressed to:

Head of the Department of Mechanical Engineering
University of Saskatchewan
Saskatoon, Saskatchewan, S7N 5A9

ABSTRACT

Previous studies show that the Piezoelectric-Driven Stick-Slip (PDSS) actuator is a promising device in many micropositioning and micromanipulation applications, where positioning with a long range and a high resolution is required. However, research in this area is still in its early stage and many issues remain to be addressed. One key issue is the representation of the dynamic displacement of the end-effector. It is known that such factors as the dynamics of piezoelectric actuator (PEA) and the presliding friction involved can significantly contribute to the displacement dynamics. Although this has been widely accepted, specific quantitative relationship between the aforementioned factors and the displacement dynamics has rarely been defined. The aim of this research is to develop a model to represent the displacement of the end-effecter of the PDSS actuators, in which both the presliding friction and the PEA dynamics are addressed.

In order to represent the presliding friction, the models reported in literatures, including Dahl model [Olsson, *et al*., 1998], Reset Integrator model [Haessig and Friedland 1991], LuGre model [Canudas de Wit *et al*., 1995] and Elastoplastic model [Dupont *et al*., 2002] were reviewed and examined; and the LuGre model was chosen to be used because of its efficiency and simple formulation. On the other hand, a linear second order dynamic system model was employed to represent the combination of a PEA and its driven mechanism. On the basis of the pre-sliding friction model and the linearized PEA dynamics model, a model representative of the end-effector displacement of the PDSS actuator model was developed.

In order to validate experimentally the developed PDSS model, a displacement measuring and data acquisition experiment system was established and a prototype was developed based on dSPACE and Simulink. On the prototyped actuator, two experiments were designed and conducted to identify the parameters involved in the model. One experiment is for the determination of the parameters of the second order system for the dynamics of the combination of a PEA and its driven mechanism; and other one is for the determination of the parameters of the chosen friction model. The identified parameters were then employed in the developed PDSS model to simulate the displacements and the results were compared with the experimental results that were obtained under the same operating conditions as the simulation. The comparison suggests that the model developed in this study is promising for the end-effector displacement of the PDSS actuator.

ACKNOWLEDGMENTS

At First, I would like to give my sincere gratitude to my supervisor Professor Daniel X. B. Chen for his support and the dedication to this research work which help me make progress. His invaluable suggestion, guidance and encouragement not only drive me to fulfill present research project but will also benefit me for my further work.

I also wish to deliver my sincere appreciation to Professor Chris W. J. Zhang and Professor Reza Fotouhi for being my advisory committee members. Meanwhile, my earnest gratitude goes to Professor Allan Dolovich, Professor Richard Burton and Professor David Torvi for their precious advices and thoughtful consideration from the beginning of my study. Besides, my appreciation goes to Professor Carey Simonson, Professor David Summer, Professor James Bugg and Professor Walerian Szyszkowski, Ms. April Witteg, Mr. Doug Bitner and Mr. Hans Steinmetz. Without their kindness my study couldn't work out.

The financial support from Mechanical department is truthfully acknowledged.

Finally, special thanks are given to my friends and everyone helping me to achieve this project and make this period of time in University of Saskatchewan becoming the most wonderful one in my memory.

TO MY MOTHER WANG, YIWEN AND MY FATHER KANG, JINGLIANG

献给我的母亲王毅文和我的父亲康景良

TABLE OF CONTENTS

page

LIST OF TABLES

LIST OF FIGURES

LIST OF ABBREVIATIONS

ABBREVIATION	
A	true area of contact surface, m^2
$ADC\#1Input$	ADC input voltage of the DS1102 control board, V
$a(z)$	parameter of the stiction magnitude determination
C	steady state gain
c	damping ratio of the combination of the PEA and the stage, kg/s
c_s	stage damping coefficient, kg/s
c_m	$c_m = c/m$, kg/s
D	displacement to voltage proportion of piezoelectric actuator, $\mu m/V$
E	force to voltage proportion of for piezoelectric actuator, N/V
F_C	Coulomb friction, N
F_e	external force, N
F_f	friction force, N
F_N	normal force, N
F_p	force generated by the piezoelectric actuator, N
F_s	interaction force between the PEA and the stage, N
F_{ST}	stiction, N
$F(v)$	friction force as a function of velocity, N
$G(s)$	transfer function of the PEA and the stage system

k	stiffness of the combination of the PEA and the stage, kg/s^2
k_m	$k_m = k/m$, kg/s^2
k_s	stage stiffness, kg/s^2
L	full length of a material, μm
$L1$	length of the PEA before elongation, μm
m	mass of the PEA and the stage, kg
m_e	mass of the end-effector, kg
m_s	stage mass, kg
$OS\%$	overshoot of step response, %
PEA	piezoelectric actuator
PDSSA	piezoelectric-driven stick-slip actuator
$PZT3$	length of the PEA after elongation, μm
r^2	coefficient of determination
s	shear force per unit area of junctions, N/m^2
$\text{sgn}(F_e)$	sign of F_e
$\text{sgn}(v)$	sign of the velocity
T	electrical-mechanical transformer ratio, N/V
T_m	$T_m = T/m$, N/Vkg
T_p	peak time of step response, s
T_r	rising time of step response, s
T_s	settling time of step response, s

$U(s)$	voltage input in frequency domain
u_{ss}	steady state input voltage, V
u	voltage signal applied to the PEA, V
v	velocity of a sliding object, $\mu m/s$
w	plastic (irreversible) displacement of friction, μm
$\dot{w}$	velocity of the plastic deformation, $\mu m/s$
x	displacement of friction, μm
$\dot{x}$	velocity of a sliding object, $\mu m/s$
x_C	displacement sensor output before the calibration, μm
x_e	displacement of the end-effecter, μm
$Y(s)$	displacement output in frequency domain
y	displacement of the stage, μm
y_C	displacement sensor output after the calibration, μm
y_{ss}	steady state displacement of the stage, μm
z	elastic (reversible) displacement of friction, μm
$\dot{z}$	velocity of the elastic deformation, $\mu m/s$
z_{ss}	steady state elastic displacement, $\mu m/s$
z_0	breakaway displacement, $\mu m/s$
α	parameter of the stress-strain relation determination
$\alpha(z,\dot{x})$	piecewise continuous function of the Elastoplastic friction model
$\alpha_m(\cdot)$	$\alpha(z,\dot{x})$ if $z_{ba} \le \lvert z \rvert \le z_{ss}(\dot{x})$

ΔL	deformation or the change in length of a material, μm
ΔV	voltage difference applied to the piezoelectric actuator, V
ΔX	expanding displacement of piezoelectric actuator, μm
ε	strain
ζ	damping ratio
μ	coefficient of friction
σ_0	coefficient of the contact stiffness, kg/s^2
σ_1	damping coefficient of the tangential compliance, kg/s
σ_2	parameter of the viscous friction, kg/s
ω_n	natural frequency, rad/s

CHAPTER 1 INTRODUCTION

1.1 Piezoelectric Actuators

An actuator is a mechanical device for moving or controlling a mechanism or system. Generally, an actuator can be electric, hydraulic, or pneumatic by employing, electric, hydraulic, or pneumatic signals or energy, respectively. Actuators have been widely used in various engineering applications. In some of the applications, people are doing work on small scale mechanism, and they are very concerned with the precision of the actuator's movement. In microscopic surgical operations, for example, using a needle to puncture the wall of a cell is a common practice, and the depth that the needle reaches into the cell is vital to this operation, which typically requires that the displacement of the needle is controlled in a range of several millimeters with a resolution of a few micrometers or even in submicron. Similar long range and fine resolution applications are found in precision mechanical engineering [Pohl, 1987; Chang and Li, 1999], the manipulation of biological sample [Bergander, 2003], minimally invasive surgery [Edinger *et al*., 2003], scanning microscopy [Meyer *et al*., 2005], etc.

In the past, in order to achieve smoothly positioning with high resolution and long range, the typical micromanipulators were made up with hydraulic actuators, electrical motor actuators or the combination of them. The hydraulic micropositioner is good at preventing vibration and for

providing force, but it usually performs well only in low actuation frequency and is heavy in weight. The electrical motor micropositioner is usually custom designed combining with roller bearing slides. This kind of micropositioner is also heavy and consumes significant electric power. [Bergander et al., 2003; Niezrecki et al., 2001] The piezoelectric related actuator is another way to realize micropositioning and micromanipulating. Among existing precision positioners including the hydraulic micropositioners and the electrical motor micropositioners, the piezoelectric related actuators hold the most promise for the aforementioned applications.

The working principle of a piezoelectric actuator (PEA) is based on the piezoelectricity effect, which was first discovered by Pierre and Jacques Curie in 1880s. When a stress is applied to a piezoelectric material such as a crystal, it produces an electrical voltage proportional to the magnitude of the stress. The piezoelectric effect is reversible in that a piezoelectric material, when subjected to an applied voltage, can change its shape or dimension proportional to the applied voltage. Microscopically, the unit cell of piezoelectric crystallites with polarization and deformation exhibits electrical and mechanical asymmetry. When a voltage is applied to the poled crystallites, ions in the unit cells are shifted. The displacements of these shifted ions are summed up becoming the dimensional deflection of the piezoelectric crystallites. For a natural crystal material, the dimension change is too small to be applied in engineering, even if a high voltage is applied. As a result, a number of piezoelectric ceramic wafers are often stacked together to build an actuator. With interleafed with electrodes, as schematically shown in Figure 1.1, the stacked piezoelectric ceramic wafers are connected in series mechanically and connected in parallel electrically. Since the wafer is thin, the positive electrode is close to the negative electrodes, and the expansion of each thin piezoelectric wafer is added up to generate a

considerable displacement. Consequently, the useful expansion of the stacked piezoelectric material could be obtained by applying a modest voltage on the stack. Since the piezoelectric stack actuators are monolithic and have no sliding or rolling parts, they don't have the mechanical stiction or backlash, which other actuators usually exhibit. Besides, they can perform step movements with a resolution in nanometer scale, has bandwidth on the order of kilohertz, and are able to provide mechanical power on the order of several watts [Goldfarb and Celanovic, 1997]. Thus, PEAs are well suited for use in various precision positioning and micromanipulation applications.

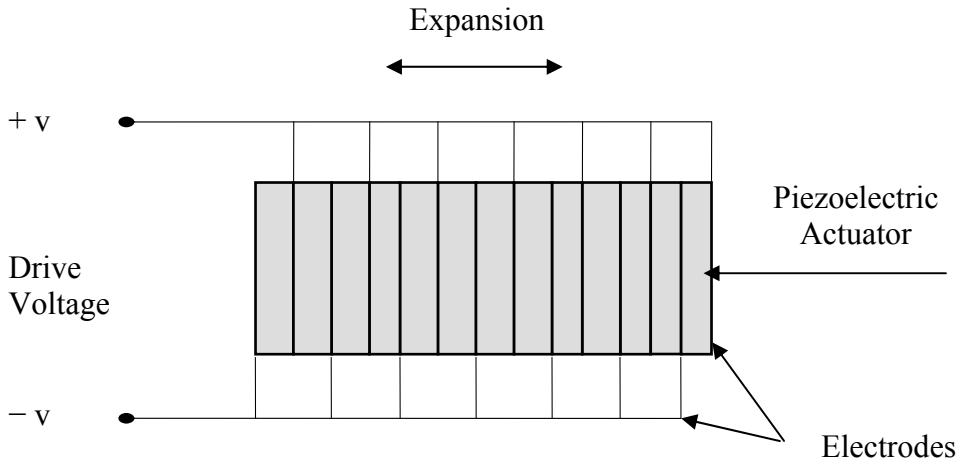

Figure 1.1 Schematic Representation of a Piezoelectric Stack

Piezoelectric actuators have been becoming the prevailing mechanical device in many engineering applications, especially in small scale mechanism operations and manipulations. It is reported [Adriaens *et al*., 2000] that, nowadays, the PEA is commercially available for producing displacements in the range of 10 pm (1 pm = 10^{-12} m) to 100 μm. However, the displacement range of the PEA is small although its resolution is favorably fine. The small displacement range

of its elongation greatly limits the applications of the PEA. In many micromanipulator applications, it is expected that the slider of a manipulator is able to move in a range over a few millimeters with a high resolution. For instance, if the PEA is employed in the cell manipulation, which is the aforementioned example, the fine resolution and the good force provision of the PEA is favorable in the cell injection, but its small displacement range limits it making further more flexible motion, e.g. moving the needle from some millimeters away to the cell. The limited displacement range is the drawback of the PEA or the PEA stack. To increase the displacement range of a PEA, meanwhile maintaining its fine resolution, is the motivation of the present study.

1.2 Piezoelectric-Driven Stick-Slip Actuators

One straightforward method for a longer displacement range is to have an amplification mechanism connected to a piezoelectric actuator. However, due to the limited amplifying factor, the amplified displacement is also challenged by the demand of long-range positioning. Moreover, an increase in displacement in this manner is at the cost of a decrease in output force. In addition to the use of amplifying mechanism, actuators based on the concept of inchworm, which was developed and patented by Burleigh Instrument in the 1970s, have been widely recognized for increasing displacement range [Tenzer and Mrad, 2004; Niezrecki *et al*., 2001]. An inchworm actuator typically consists of three or more actuation elements; one element is used to generate longitudinal extension or the actuator's displacement and two or more elements for the clamping and guiding function. The distinct characteristics of inchworm actuators are the well-defined step size and considerably-increased range of displacement (only limited by the

length of the guideway used). The main drawback is the use of at least three actuation elements, thereby significantly increasing the system complexity and cost.

Another similar paradigm for increasing displacement range is based on the concept of friction-inertia or inertial sliding [Pohl, 1987]. This concept is illustrated in Figure 1.2. In Figure 1.2 (a), an end-effector (object 3) is supported and guided by a movable platform (object 2) which is driven by a piezoelectric element (object 1). During the course of a slow expansion of the piezoelectric element, the end-effector moves along with the platform if the friction between the end-effector and the movable platform is larger than the force due to inertia, as shown in Figure 1.2 (b). However, if the piezoelectric element suddenly contracts and the inertial force becomes larger than the friction, the end-effector will slide on the platform in Figure 1.2 (c). As a result, the end-effector moves a step Δs with respect to its original position. By repeating the process, the Object 3 will move continuously. Thus, a theoretically-unlimited displacement with a high resolution can be achieved. In the Figure, s_0 is the displacement of the end-effecter moving to the right. It can be seen that only one actuation element is required for such a stick-slip actuator, leading to simple structure and small size. However, it should be noted that the output force becomes limited, which is depending on the `friction between the end-effector and the movable platform. Even though, the stick-slip actuators have still found its wide applications, where the critical issue is not the output force but the displacement capability, such as in the fields of scanning microscopy, micro robotics, and microsystems [Bergander *et al.*, 2003; Pohl, 1987; Renner *et al*., 1990; Chang and Li, 1999; Hoogeman *et al*., 1998; Zhang *et al*., 2006].

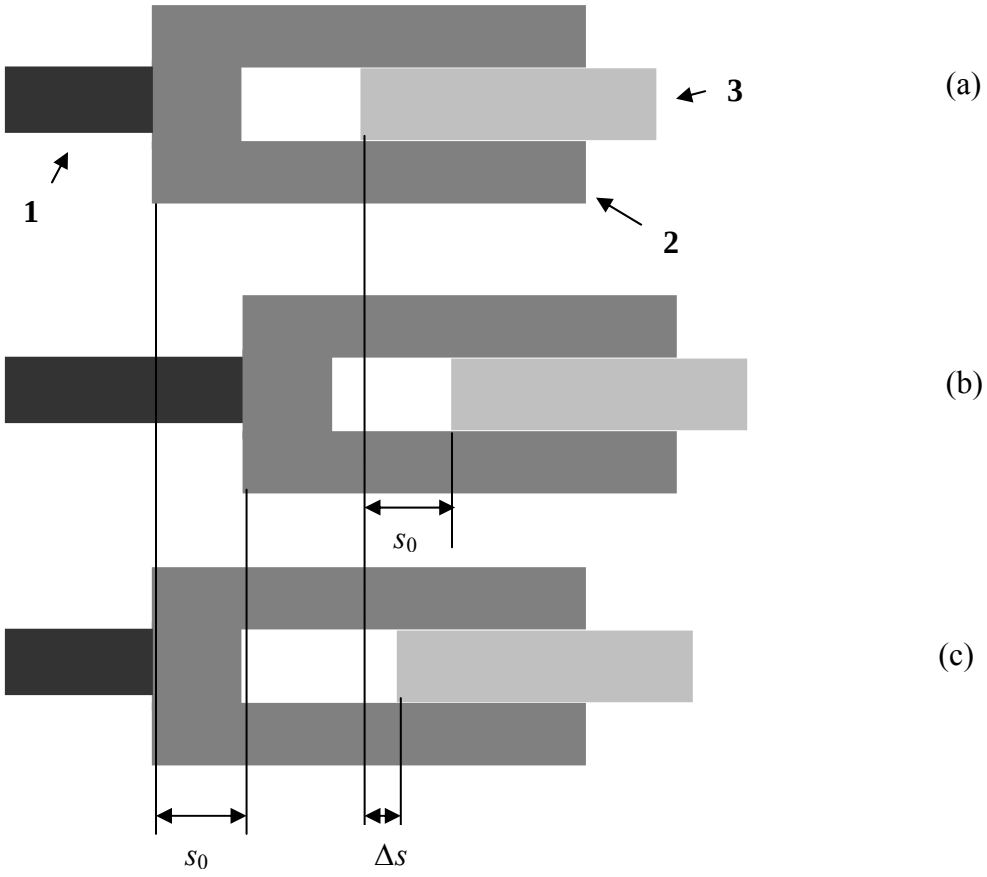

Figure 1.2 Inertia Sliding Principle

Although actuators designed based on the above inertia sliding concept, which is called piezoelectric-driven stick-slip (PDSS) actuators in this study, hold the remarkable advantage to other actuators, research in this field is still in its early stage and many issues remain to be addressed. One of the key issues could be the modeling of the dynamics of such an actuator, i.e., the representation of the displacement of end-effector. It is known that some factors can have significant influence on the performance of actuator, such as the voltage signals (including its waveform, magnitude and frequency) applied to the actuator, the geometries and the masses of the components of the actuator, and the friction force presented between Object 2 and Object 3, as shown in Figure 1.2. Although this has been widely accepted, specific quantitative

relationship between the aforementioned factors and the actuator performance has rarely been defined. Recently, only a few studies investigated this relationship, which are reviewed in following section, along with the limitations of these studies.

1.3 Previous Studies on Modeling of Piezoelectric-Driven Stick-Slip Actuators

In the modeling of piezoelectric-driven stick-slip (PDSS) actuators, the early remarkable work was contributed by Pohl [Pohl, 1987], followed by the one by Chang and Li [Chang and Li, 1999]. Both studies are reviewed in this section.

In Pohl's study, a PDSS actuator was designed and developed, which is shown schematically in Figure 1.3 [Pohl, 1987]. In the figure, the load 1 and translation stage 2 rides on translation support 3 and they can slide between A and B. Piezoelectric tube 7 is fixed firmly between base 6 and support 3 which is clamped by elastic plates 4 and 5. In test, the saw-tooth voltage signal is applied to the piezoelectric tube, and it pushes the support 3 moving back and forth. The working principle is the same as the one of the PDSS actuator described previously. The load 1 and translation stage 2 will slide step by step under the friction between stage 2 and support 3, and thus the displacement of load 1 will increase continuously. In this actuator, the displacement of the piezoelectric actuator is amplified by using two elastic spring-like plates. It is reported [Pohl, 1987] that the step size of the actuator could be 0.04 - 0.2 μm, and that the speed of the moving part could be 0.2 mm/s.

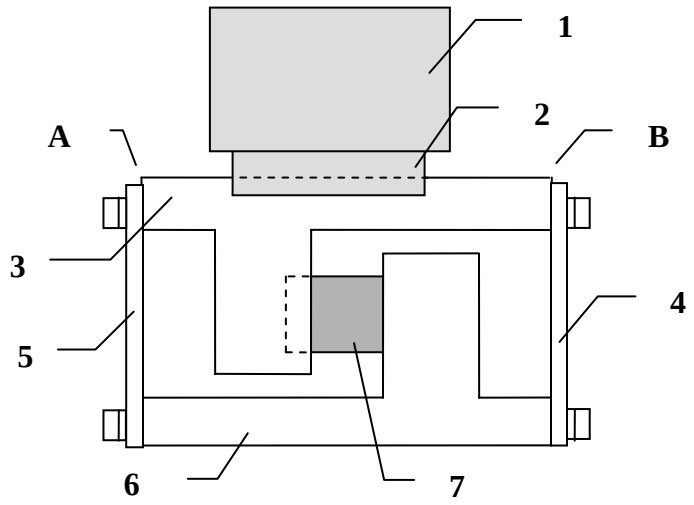

Figure 1.3 Schematic of a PDSS actuator developed by Pohl [Pohl 1987]

In the Pohl's study, the PEA was simplified as a simple linear component, and the relationship between the PEA actuation or displacement of PEA and the driving voltage was represented by using a linear function. Specifically, the displacement and the force generated are related to the voltage applied to the PEA by the following equations [Pohl, 1987].

$$\Delta X = D \times \Delta V \tag{1.1}$$

$$F_p = E \times \Delta V \tag{1.2}$$

where ΔX is the expanding displacement of piezoelectric actuator, F_p is the force generated by the piezoelectric actuator; ΔV is the voltage difference applied to the piezoelectric actuator; and E and D are coefficients, relating the voltage to the force and the displacement, respectively.

It is noted that the above model does not include the PEA dynamics as well as the influence of the friction nonlinearity.

Another study related to the modeling of the PDSS actuator was reported by Chang and Li [Chang and Li, 1999]. The schematic diagram of their actuator is shown in Figure 1.4, in which M is the mass of the movable stage; m the mass of the slider or end-effecter; k stiffness of the spring; and c damping of the damper. In this work, the friction between the slider and movable platform is represented by using the Coulomb friction, and the dynamics of the piezoelectric actuator is modeled and equivalent to the one of a mass-spring-damping system. Based on the developed model, Chang and Li also carried out simulations to investigate the actuator performance, with different waveforms of the voltage applied to the piezoelectric element. Apart from the necessity of experimentally validating the simulation results, it should be noted that the use of the Coulomb fiction model to represent the friction in such a stick-slip actuator may not be appropriate. Since in a small motion (typically several microns), the friction is dominated by the presliding displacement, i.e., the motion prior to fully developed slip, and its nature is inherently different from the Coulomb fiction [Dupont, 2002; Ferretti, 2004]. This situation raises a need to develop an improved model for the piezoelectric-driven stick-slip actuator, in which the presliding friction and the dynamics of the PEA are considered.

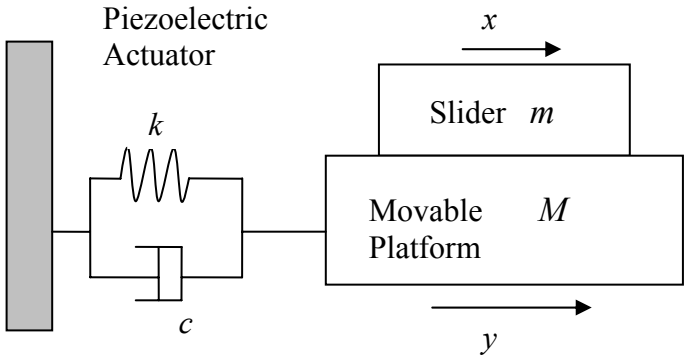

Figure 1.4 Schematic of a PDSS actuator reported by Chang and Li [Chang and Li, 1999]

1.4 The Research Objectives

To meet the aforementioned need, the objective of this research project is to develop a model to represent the dynamics of the motion of the end-effecter of the PDSS actuator, in which both the dynamics of the PEA and presliding friction are included. To achieve this objective, the following research activities are to be conducted in this research.

(1) Develop a model to represent the dynamics of the displacement of the end-effector of the PDSS actuator, taking into account the dynamics of the PEA and presliding friction.

(2) Design and develop a prototype of the PDSS actuator as well as a displacement measuring and data acquisition system for the purpose of testing the developed model.

(3) Verify the effectiveness of the developed model by measuring the dynamics of displacement and then comparing it to the one simulated from the model.

1.5 Organization of the Thesis

This thesis consists six chapters, including this chapter. Other chapters are briefly described as follows.

CHAPTER 2 Modeling of the Friction

This chapter deals with modeling of the friction that is dominated by the presliding displacement, which is of particular interest in this research. In particular, the models reported in literatures, including Dahl model; Reset Integrator model; LuGre model and Dupont model are reviewed and examined.

CHAPTER 3 Modeling of PDSS Actuators

By considering the PEA and the stage supporting the end-effect as a standalone system, modeling of its dynamics is addressed in this chapter. On this basis, a model representative of the displacement of the end-effector in a PDSS actuator is developed, in which both the dynamics of the PEA and presliding friction are included.

CHAPTER 4 Experimental Setups

In this chapter, the displacement measuring and data acquisition system designed and developed in this research is presented, along with the principles behind and the functions of the main components used in the system. Also, presented in this chapter is a prototype design of a PDSS actuator as well as the calibration of a displacement sensor used in this research.

CHAPTER 5 Experimental Verification

In this chapter, the experiments are carried out on the experiment system described in Chapter 4 and their results are presented for the model verification. In one experiment, the parameters of the piezoelectric actuator and stage are estimated as an independent system. The results obtained from another experiment are used to identify the parameters involved in the developed PDSS actuator model, including the parameters of the friction model. With the PDSS actuator model determined, its effectiveness is validated by comparing them to the results simulated from the model.

CHAPTER 6 Conclusions and Future Work

This chapter presents the conclusions drawn from this research, which is followed by the suggestion for possible future work.

CHAPTER 2 MODELING OF FRICTION

2.1 Introduction

By definition, friction is the resistance to the relative motion of one body sliding, rolling or flowing over another with which it is in contact. Friction exists in all mechanical systems, e.g., bearings, transmissions, hydraulic and pneumatic cylinders, valves, brakes and wheels [Olsson *et al.*, 1998]. In control engineering, friction is an important issue to be addressed. Friction causes unwanted vibration and weariness, as well as unexpected error in analysis due to the inaccuracy of its modeling. While striving to reduce friction in the aforementioned mechanical systems, people are also working to utilize friction in the cases where friction is a driving force, such as in the PDSS actuators considered in this research. To model the PDSS actuator, one of the important steps is to represent the friction involved in the actuator. In this chapter, the previous studies on friction and various friction models developed are reviewed and examined.

2.2 Classical Modeling of Friction

Discovery and application of friction can likely be traced back to the pre-history time. But it was much later that the scientific or academic investigation to the friction was carried out. In the

middle of fifteen century, Leonardo da Vinci first introduced the two basic friction laws. The first law of friction states that the friction is proportional to the normal force applied on the contact surfaces; and the second one says that the friction is irrelevant to the area of the contact surfaces. A quite different view of friction is proposed by Desaguliers in 1734. He observed the adhesion plays a very important role in friction in his experiment and concluded that the larger area of contact surfaces results in the bigger friction. However, this was rejected by Charles Augustin Coulomb in 1781. Coulomb proposed that the adhesion may play some role in friction but the roughness of the contact surfaces is primary to cause friction. This "roughness hypothesis of friction" theory coincides with the two aforementioned friction laws [Bowden and Tabor, 1973]. From the above discussion, it is seen that, the early researchers noticed the various aspects of friction phenomena, and also developed the friction laws for use in friction analysis. However, a lot leaves to be desired. With the advance in experiment techniques and the development of the relevant physics theories, the improvement of the understanding on friction became possible and various models and theories were developed.

In the 1940s, Holm, Ernst and Merchant, Bowden and Tabor found that there is a great difference between the geometrical area of contact and the real area of contact which is formed by the touching asperities of the contact surfaces [Czichos, 1978]. The atoms of these asperities on one contact surface are very close to the atoms on the other contact surface so that they attract each other and become junctions. Force is required to break these junctions or the attractions from both tangential and normal directions. Particularly, the tangential force is regarded as the friction. Instinctively, it is seen that the junctions in static state are more difficult to be broken. As a result, the static friction is greater than sliding friction. The junction theory also accounts

for the adhesion effect of the contact surfaces, which gives reliable reason to compromise Desaguliers and Coulomb's observation. The contact asperities have both plastic deformation which causes the adhesion or viscous friction and elastic deformation the dominate force of friction.

In the classical models of friction, the term of Coulomb friction is usually used and has the form of

$$F_C = \mu F_N \tag{2.1}$$

Where F_C is Coulomb friction; F_N is the normal force; and μ is the coefficient of friction. As shown in Figure 2.1 a), the Coulomb friction can be depicted in that, upon the application of an external force to generate the relative motion between the contacted surfaces, the friction between them occurs and jumps to the Coulomb friction if the external force is big enough. The friction will then keep a constant regardless the variation of the velocity of the relative motion. Obviously, this representation does not include the static friction and viscous friction effect.

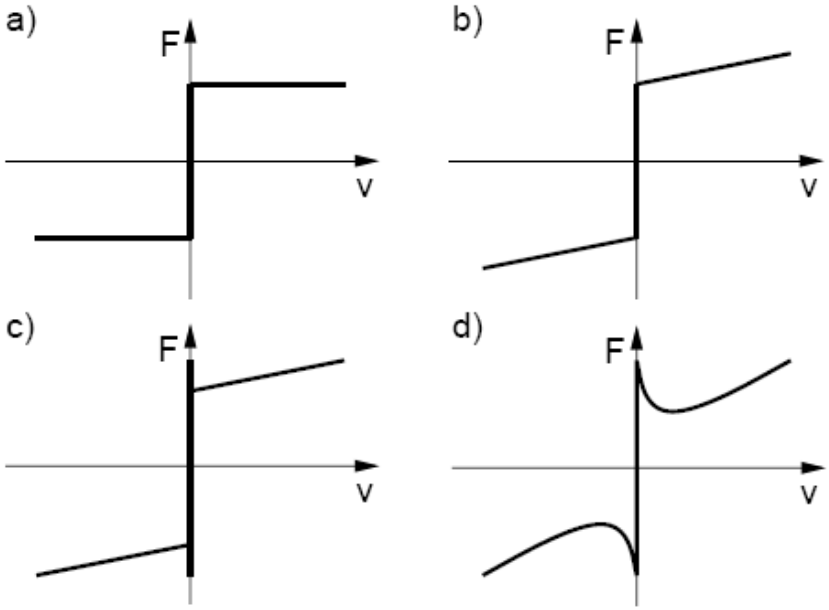

Figure 2.1 Representations of friction; a) Coulomb friction, b) Coulomb plus viscous friction, c) Stiction plus Coulomb and viscous friction, d) Friction with Stribeck effect [Olsson, 1998]

In fact, there are some assumptions made in the Coulomb friction. These assumptions include that the real contact area keeps the same all the time and that the shear force of the junction on a unit area of the contact surface is constant. To release these assumptions, Bowden and Tabor [Bowden and Tabor, 1973] used the following form for the friction representation.

$$F_f = A \cdot s \tag{2.2}$$

where F_f is the friction; A is the true area of contact surfaces; s is the shear force per unit area of junctions. If the adhesion or viscous friction is considered, both the true area of contact surfaces

A and the shear force s will change, depending on the velocity of relative motion. As a result, the friction force increases with velocity, as illustrated in Figure 2.1 b). In other words, once the object starts to move under an external force, the friction is not a constant but a function of velocity.

In the literature, stiction is a short term for the static friction between two contacted surfaces, when there is no remarkable relative motion between them. Figure 2.1 c) shows the friction versus the velocity, in which the stiction and viscous friction is considered. In 1902, Stribeck observed and argued that the friction force does not decrease discontinuously at low velocity as shown in Fig 2.1 c), instead that the velocity dependence of friction is continuous as shown in Fig 2.1 d). This is named Stribeck effect [Olsson, 1996]. Under Stribeck effect the friction starts from zero to stiction at zero velocity, and then decreases continuously with the increasing velocity at low velocity. After that, the friction will increase as the velocity increases. The general expression of the classical friction is given as following [Olsson, 1996].

$$F_f = \begin{cases} F(v) & if\ x \neq 0 \\ F_e & if\ v = 0\ and\ |F_e| < F_S \\ F_S \operatorname{sgn}(F_e) & otherwise \end{cases} \tag{2.3}$$

where F_e is the external force applied to the object; F_S is the stiction; $F(v)$ is a function of velocity or a constant.

The above models are classified into classical or static models, in which the velocity is assumed steady. For this research project which focuses on dynamics system response and the

displacement output of the PDSS actuator is in micrometers or less and the end-effecter is always under the motion prior to the fully developed slip, these classical models may not adequate to represent the presliding friction which is concerned to simulate the transferring phase between sticking and sliding. The review of modeling of the presliding friction is provided in the following section.

2.3 Pre-sliding Friction and Displacement

Pre-sliding friction is referred to the friction happening in the motion prior to the fully developed slip. The displacement of pre-sliding friction usually extends less than a few micrometers. In this regime, the characteristics of the friction differ from the one in other friction regimes, in that the friction is a function of displacement [Dupont *et al*., 2002]. Rabinowicz pointed out that the presliding displacement is an elastic displacement, taking place between the contact surfaces before sliding commences [Rabinowicz, 1951].

Along with a different avenue, Bowden and Tabor [Bowden and Tabor, 1973] suggested that the microscopic contact surfaces of objects can be considered having a number of asperities, as illustrated in Figure 2.2. When either a normal or a tangential force is applied, the asperities on one contacted surface are pressed towards the asperities on the other contact surface; and both elastic and plastic deformations occur in these asperities. In the literature [Olsson, 1996], these contacted asperities are modeled as elastic bristles that are deflecting as springs, generating forces opposite to the tangential component, and the resultant force is the friction force. Figure 2.3 shows one of the deflected bristles. For modeling the friction force, all of the bristles can be

simply represented by using a single bristle with the average stiffness of all the bristles, based on the superposition property that the linear bristle have.

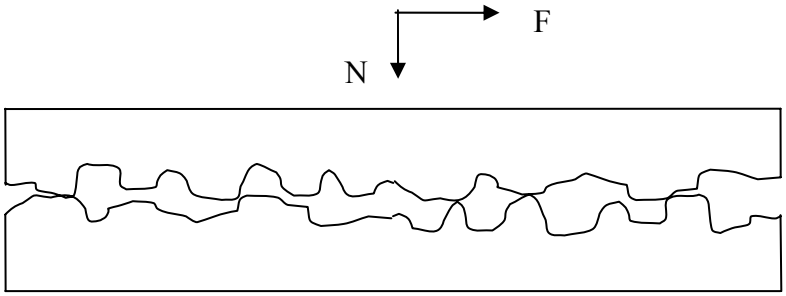

Figure 2.2 Microscopic illustration of friction contact [Olsson, 1996]

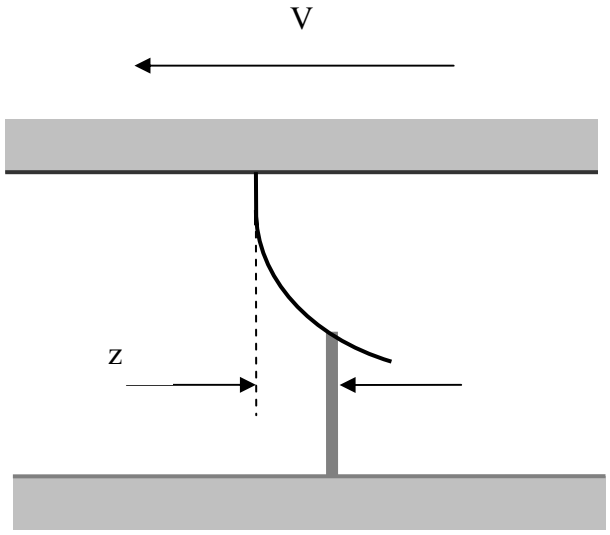

Figure 2.3 Deflected bristle [Olsson, *et al*., 1998]

The pre-sliding friction is also called elastoplastic friction; and its displacement can be categorized into the following phases: elastic displacement; mixed elastic & plastic displacement; and plastic displacement [Dupont, *et al*., 2002]. In any of these phases, the displacement occurring in the presliding period, denoted by x, can be decomposed into the elastic (reversible) and the plastic (irreversible) components, denoted by z and w respectively, i.e.

$$x = z + w \tag{2.4}$$

On this basis, the aforementioned three phases of the presliding are characterized with the following velocity equations, respectively.

$$\text{Elastic} \qquad \begin{cases} \dot{x} = \dot{z} \\ \dot{w} = 0 \end{cases} \tag{2.5}$$

$$\text{Mixed elastic and plastic} \qquad \dot{x} = \dot{z} + \dot{w} \tag{2.6}$$

$$\text{Plastic} \qquad \begin{cases} \dot{x} = \dot{w} \\ \dot{z} = 0 \end{cases} \tag{2.7}$$

In the elastic phase, the velocity of object equals to the one of the elastic deformation, i.e. $\dot{x} = \dot{z}$, while the velocity of the plastic sliding is $\dot{w} = 0$. In mixed elastic and plastic phase the velocity of object equals to the sum of the velocities of the elastic deformation and the plastic sliding, i.e. $\dot{x} = \dot{z} + \dot{w}$. In slipping phase, the velocity of object equals to the one of the plastic sliding, i.e. $\dot{x} = \dot{w}$, and the one of the elastic deformation $\dot{z}$ is 0. Based on the elastic and plastic

displacement concept, various models were reported in literature to represent the pre-sliding friction, which are outlined in the following section.

2.4 Modeling Pre-sliding Friction and Dynamics

As mentioned previously, the classical models reviewed in **§ 2.2** are not able to represent the presliding friction, which, however, is of particular interest in this research. Driven by this need, various models reported in the literature to represent the presliding friction and its dynamics were reviewed and examined by the author; and four of these models are outlined in this section. These four models are the Dahl model, Reset Integrator model, LuGre model and Elasoplastic model, which are to be adopted and used in this research.

2.4.1 Dahl Model

In 1968, Dahl adopted the concept of the strain and stress relationship from classical solid mechanics and modeled friction by using a differential equation. On this basis, the friction force is considered as only position dependent, taking the following form [Olsson, *et al*., 1998]

$$F_f = \sigma_0 \cdot z \tag{2.8}$$

$$\frac{dF_f}{dx} = \sigma_0 \left(1 - \frac{F_f}{Fc} \operatorname{sgn} v \right)^{\alpha} \tag{2.9}$$

where F_f is the friction force, z the elastic component of the displacement, x the displacement, F_C the Coulomb friction force, $\dot{x}$ the relative velocity between the two friction surfaces, σ_0 the stiffness coefficient, and α a parameter to determine the shape of the stress-strain curve in friction and, typically, takes a value of 1 in the literature. In the time domain, the above Dahl model can also be expressed as

$$\frac{dF_f}{dt} = \frac{dF_f}{dx} \cdot \frac{dx}{dt} = \sigma_0 \cdot \dot{x} \left(1 - \frac{F_f}{Fc} \operatorname{sgn} \dot{x} \right) \tag{2.10}$$

Substituting (2.8) into (2.10), one has

$$\dot{z} = \dot{x} \left(1 - \frac{F_f}{Fc} \operatorname{sgn} \dot{x} \right) \tag{2.11}$$

It is noted in the above Dahl model that the friction is represented by a linear function of the displacement. This coincides with the representation of the friction in the previously-reviewed bristle model, i.e. $F_f = \sigma_0 \cdot z$, in which σ_0 and z are the stiffness and the deflection of the bristle, respectively.

The Dahl model has the advantage in its simple form and, due to this, it has been extensively used in various modeling applications [Haessig and Friedland 1991; Bliman 1992]. On the other hand, due to its simplicity, the Dahl model is not able to describe the viscous friction, stiction,

and Stribeck effect. To alleviate this problem, researchers have been trying to improve it, resulting different models. One of the models is the reset integrator model.

2.4.2 Reset Integrator Model

The Reset Integrator Model was developed by Haessig and Friedland [Haessig and Friedland 1991]. In this model, the stiction and viscous friction are considered, different from the Dahl model. This model also utilizes the bristle assumption, i.e. the use of a single bristle to represent the contact between two surfaces. Particularly, the strain and displacement are not separated variables in reset integrator model, instead strain and displacement is denoted by using a single variable which has different values in different interval. The Reset Integrator Model takes the following form [Haessig and Friedland 1991].

$$\dot{z} = \begin{cases} 0 & if\left(v > 0 \; and \; z \geq z_{ba}\right) or \left(v < 0 \; and \; z \leq -z_{ba}\right) \\ v & \text{otherwise} \end{cases} \tag{2.12}$$

$$F = \left(1 + a(z)\right) \cdot z \cdot \sigma_0(v) + \sigma_2 \dot{z} \tag{2.13}$$

In this model, a breakaway displacement, denoted by z_0, is introduced by assuming that only the elastic displacement occurs if $|z| < z_0$. Besides, the Coulomb friction is represented by $z \cdot \sigma_0(v)$ where z represents strain, v is the velocity, which is the same as Dahl model's expression; and

the stiction overshoot is represented by $a(z)\cdot z\cdot \sigma_0(v)$, in which $a(z)$ takes the form of [Olsson *et al*., 1998]

$$a(z)=\begin{cases} a & if\ |z| < z_0 \\ 0 & otherwise \end{cases} \tag{2.14}$$

where a is a constant, determining the magnitude of stiction. Once the displacement reaches the breakaway one, i.e. $z = z_0$, the stiction overshoot becomes zero. In (2.13), the term of $\sigma_2\dot{z}$ denotes the viscous friction.

The improvement of Reset Integrator Model over the Dahl model is that the stiction and viscous friction is considered. However, it is discontinuous on the breakaway point, i.e. it is not able to include Stribeck effect. Furthermore, in Reset Integrator model the displacement increases linearly with respect to stiction prior to reaching the breakaway displacement; and also the nonlinearity of the pre-sliding friction is neglected. Besides, people are easy to be confused by employing one single variable describing the elastic deformation and the plastic deformation at the same time in Reset Integrator model.

2.4.3 LuGre Model

The LuGre model takes into account the stiction, the viscous friction, and the Stribeck effect simultaneously, which is given by [Canudas de Wit *et al*., 1995]

$$\dot{z} = v\left(1 - \frac{\sigma_0}{|Fc|}\operatorname{sgn}\dot{x}\cdot z\right) \tag{2.15}$$

$$F = \sigma_0 \cdot z + \sigma_1 \cdot \dot{z} + \sigma_2 \cdot \dot{x} \tag{2.16}$$

where σ_0 the contact stiffness, σ_1 the damping of the tangential compliance, and σ_2 the coefficient of viscous friction are positive coefficients. It is seen that, in the LuGre model, the stiction overshoot is included by introducing the damping terms of $\sigma_1\dot{z}$ and $\sigma_2\dot{x}$. This is the difference between LuGre model and Dahl model. Also, it is found in the present study that these damping terms can help to significantly reduce the oscillation in the simulation results, which are to be discussed later on.

In the elastic phase of the presliding displacement, the displacement consists of only the elastic component, i.e., *z*. Therefore, one has $\dot{x} = \dot{z}$ and (2.16) is reduced to

$$F = \sigma_0 \cdot z + (\sigma_1 + \sigma_2)\cdot \dot{z} \tag{2.17}$$

2.4.4 Elastoplastic Model

An attempt to improve the LuGre model has been made by Pierre Dupont in 2002 [Dupont *et al*., 2002], resulting the elastoplastic friction model. In this model, the breakaway displacement,

denoted by z_{ba}, was introduced by assuming that only the elastic displacement occurs if $|z| \le z_{ba}$. Then, the elastoplastic friction model is described by [Pierre Dupont, 2002]

$$F_f = \sigma_0 z + \sigma_1 \dot{z} + \sigma_2 \dot{x} \tag{2.18}$$

$$\dot{z} = \dot{x}\left(1 - \alpha(z,\dot{x})\frac{z}{z_{ss}(\dot{x})}\right) \tag{2.19}$$

where σ_0, σ_1, and σ_2 are positive coefficients, and z_{ss} is the steady state value of z for a given $\dot{x}$ and $\alpha(z,\dot{x})$ is a function of z. In reference [Dupont *et al.*, 2002], $\alpha(z,\dot{x})$ is given in the following piecewise continuous function

$$\alpha(z,\dot{x}) = \left\{ \begin{array}{ll} 0, & |z| \le z_{ba} \\ \alpha_m(\cdot), & z_{ba} < |z| < z_{ss}(\dot{x}) \\ 1, & |z| \ge z_{ss}(\dot{x}) \\ 0, & \operatorname{sgn}\dot{x} \ne \operatorname{sgn} z \end{array} \right\} \quad \operatorname{sgn}\dot{x} = \operatorname{sgn} z \tag{2.20}$$

One of the possible specific functions of the $\alpha_m(\cdot)$ in (2.20) was given by Dupont as the following,

$$\alpha_m\left(z, z_{ba}, z_{ss}\right) = \frac{1}{2}\sin\left(\pi \frac{z - \left(\frac{z_{ss} + z_{ba}}{2}\right)}{z_{ss} - z_{ba}}\right) + \frac{1}{2}, \tag{2.21}$$

$$z_{ba} \le |z| \le z_{ss}(\dot{x}).$$

With the $\alpha_m(\cdot)$ given above, the piecewise continuous function $\alpha(z, \dot{x})$ was simulated by applying Simulink in Figure 2.4.

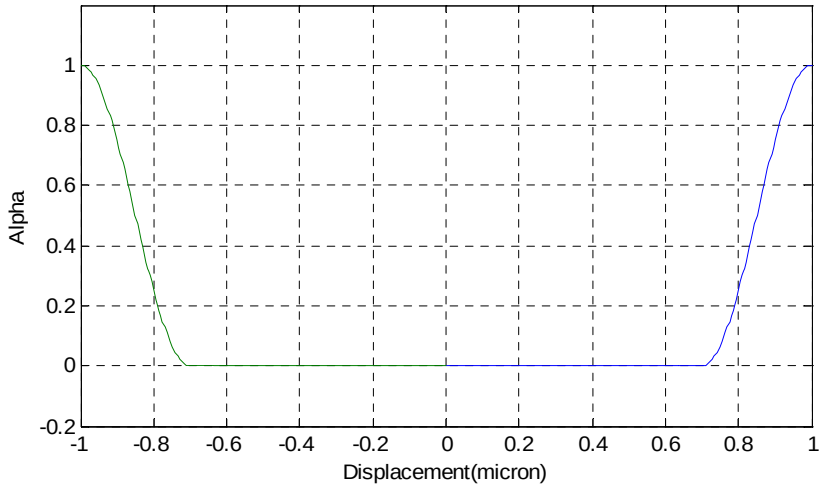

Figure 2.4 Piecewise Continuous Function $\alpha(z, \dot{x})$ of the Elastoplastic Friction Model

In the Figure 2.4, the horizontal axis is the elastic deformation of friction in micrometers, the vertical axis is the $\alpha(z, \dot{x})$, and $0 \le \alpha(z, \dot{x}) \le 1$. This plot is the graphic expression of the (2.20).

2.5 Summary

This chapter presents the review of the friction modeling. At the beginning of the chapter, various classic friction models are outlined, which is followed by the presentation of the basic concepts for pre-sliding fiction modeling, including the bristle assumption and the elastic-plastic deformation theory. Four models to represent the presliding fiction are presented and examined.

CHAPTER 3 MODELING OF THE DISPLACEMENT OF THE PIEZOELECTRIC-DRIVEN STICK-SLIP ACTUATORS

3.1 Introduction

This chapter presents the development of a model for the displacement of the piezoelectric-driven stick-slip (PDSS) actuator, which consists of two components: one of them is for modeling the pre-sliding friction and the other one for the dynamics of a combination of a piezoelectric actuator (PEA) and a stage. In particular, to represent the pre-sliding fiction involved in the PDSS actuator, the four models reviewed in the previous chapter are examined and compared in § 3.2, with the purpose of justifying the appropriate one to be used in this research. In § 3.3, by considering the PEA and the stage as a standalone system, modeling of its dynamics is addressed; and in § 3.4, by combining it with the selected pre-sliding friction model, a model representing the displacement of the end-effector in the PDSS actuator is developed.

3.2 Modeling of the Friction in the PDSS Actuator

3.2.1 Comparison between Elastoplastic Model and LuGre Model

Friction modeling is the first and vital step of the PDSS actuator modeling. Four friction models: Dahl model, LuGre model, Reset Integrator model, and Dupont's elastoplastic model, have been reviewed individually in the last chapter. Comparing these models and finding out the common features and the differences among the four models can help to select the appropriate one to be used in this research. Among these models, Dahl model has the simplest form. Because of its simplicity, Dahl model doesn't fully describe every aspect of friction, so that it is not taken into the comparison. The first two friction models to be compared are LuGre model presented in **2.4.3** and Dupont's elastoplastic friction model presented in **2.4.4**, which is followed by the comparison between LuGre model and Reset Integrator model.

The mathematical expression of elastoplastic model is given again in the following

$$F_f = \sigma_0 z + \sigma_1 \dot{z} + \sigma_2 \dot{x}, \qquad \sigma_0, \sigma_1, \sigma_2 > 0 \tag{3.1}$$

$$\dot{z} = \dot{x}\left(1 - \alpha(z, \dot{x})\frac{z}{z_{ss}(\dot{x})}\right) \tag{3.2}$$

$$\text{And} \qquad \alpha(z,\dot{x}) = \left\{ \begin{cases} 0, & |z| \le z_{ba} \\ \alpha_m(\cdot), & z_{ba} < |z| < z_{ss}(\dot{x}) \\ 1, & |z| \ge z_{ss}(\dot{x}) \end{cases} \right\} \text{sgn}\,\dot{x} = \text{sgn}\,z \qquad (3.3)$$

In equation (3.3), if $|z| \le z_{ba}$, the piecewise continuous function $\alpha(z,\dot{x}) = 0$ and $\dot{z} = \dot{x}$. Then equation (3.1) becomes

$$F_f = \sigma_0 z + (\sigma_1 + \sigma_2)\cdot \dot{z}\,, \qquad \sigma_0, \sigma_1, \sigma_2 > 0 \qquad (3.4)$$

This is same as the formulation of elastic deformation in LuGre model (2.19).

If $z_{ba} < |z| < z_{ss}(x)$ in equation (3.3), the plastic displacement starts and $\alpha(z,\dot{x}) = \alpha_m(\cdot)$. Although it is more likely to fit the curve with a special designed function $\alpha_m(\cdot)$ than applying LuGre model, the expense is scarifying simplicity.

If $|z| \ge z_{ss}(\dot{x})$ in equation (3.3), then $\alpha(z,\dot{x})$ is equal to 1. After this simplification, the elastoplastic friction model (3.2) becomes

$$\dot{z} = \dot{x}\left(1 - \frac{z}{z_{ss}(\dot{x})}\right) \qquad (3.5)$$

Because the steady state elastic deformation can be expressed corresponding to steady state velocity $\dot{x}$ as following equation [Dupont, *et al*., 2002].

$$z_{ss}(\dot{x}) = \begin{cases} \dfrac{f_{ss}(\dot{x})}{\sigma_0} & |\dot{x}| \rangle 0 \\ \lim_{\dot{x}\to 0+}\left(\dfrac{f_{ss}(\dot{x})}{\sigma_0}\right) & \dot{x} = 0 \end{cases} \tag{3.6}$$

In the above equation, $f_{ss}(\dot{x})$ is the friction with constant sliding velocity. Thus, Equation (3.5) can be rewritten to be

$$\dot{z} = \dot{x}\left(1 - \frac{\sigma_0}{|f_{ss}(\dot{x})|}\operatorname{sgn}\dot{x}\cdot z\right), \tag{3.7}$$

It is seen that, since $|f_{ss}(\dot{x})| = F_C$, (3.1) combined with (3.7) is the same as the LuGre model expression, i.e., (2.15) and (2.16). Furthermore, if $\sigma_1 = \sigma_2 = 0$ for constant sliding velocity, the LuGre model is reduced to the Dahl Model, i.e.

$$\dot{z} = \dot{x}\left(1 - \frac{\sigma_0}{F_C}\operatorname{sgn}\dot{x}\cdot z\right) \tag{3.8}$$

$$F_f = \sigma_0 \cdot z \tag{3.9}$$

If $\mathrm{sgn}(\dot{x}) \neq \mathrm{sgn}(z)$, then $\alpha(z,\dot{x})$ is zero and $\dot{z} = \dot{x}$. This is the point where the elastic displacement has the opposite direction of the object motion. This phase is expressed by providing different signs to the variables in LuGre model.

From the above discussion, it is seen that, compared to the Dupont's elastoplastic model, the LuGre model has a simpler formulation and that, if $\alpha(z,\dot{x}) = 1$, the elastoplastic model is reduced to the LuGre model.

3.2.2 Comparison between Reset Integrator Model and LuGre Model

There is also the natural interrelation between the Reset Integrator Model presented in **2.4.2** and the LuGre model in **2.4.3**. In the LuGre model, the elastic deformation is denoted by *z*. If *z* is very small, then [Haessig and Friedland 1991] [Dupont, *et al*., 2002]

$$\frac{dz}{dt} = v \tag{3.10}$$

or

$$\dot{z} = \dot{x} \tag{3.11}$$

It is seen that z is the elastic displacement of friction in LuGre model. It is known that if there is only elastic displacement, the contacted surfaces are stuck together and the fiction is stiction. Once *z* reaches its maximum, one has

$$\frac{dz}{dt} = 0 \tag{3.12}$$

$$\dot{x} = \dot{w} \tag{3.13}$$

The displacement is plastic and there is relative motion or sliding between the contacted surfaces.

In addition, the friction force given by (2.13) in the reset integrator model can be rewritten to

$$F = z \cdot \sigma_0(v) + a(z) \cdot z \cdot \sigma_0(v) + \sigma_2 \frac{dz}{dt} \tag{3.14}$$

Based on the previous analysis, the first and third items in (3.14) are exactly the same ones in the LuGre model. The only difference is the second item, which is used to represents the stiction overshoot. This stiction overshoot in the Reset Integrator model is denoted by the Coulomb friction $F = \sigma \cdot z$ times a coefficient a. By the definition of a, it has two values with respect to z. Before the breakaway point, $a(z)$ equals to a, otherwise it equals to zero. Then the stiction overshoot is a function of $\sigma_0(v)$ and z, and the frictional phenomenon that stiction is changing with velocity is indirectly represented by $\sigma_0(v)$ and z. In contrast, the stiction overshoot is directly rendered with the velocity of the elastic deformation in LuGre model. The improvement of the Reset Integrated model over the Dahl model is the use of two extra terms to represent viscous friction and stiction based on the bristle assumption of frictional contact. However, the nonlinearity of the stiction overshoot is neglected and the pre-sliding is not fully represented as the Dahl and the LuGre model. If the displacement is denoted with *x* and the elastic deformation

is still denoted with z in the Reset Integrated model, it can be seen as a simplified form of the LuGre model.

From the above comparison, it can be seen that these friction models are developed under the same bristle assumptions, and they can be applied to different applications according to their different features. Due to its simplicity and efficiency, the LuGre model, given by (2.15) and (2.16), is adopted to model the friction involved in the PDSS actuator in this research.

3.2.3 Characteristics of LuGre Model

In order to examine the characteristics of the LuGre model, several simulations are conducted by applying the LuGre model with a parabolic input, which imitates the displacement increase with time when presliding friction happens. The first simulation is shown in Figure 3.1, in which the viscous friction is assumed to be zero by letting the viscous coefficient σ_2 = 0, the contact stiffness σ_0 is chosen to be 600, the damping of the tangential compliance σ_1 is 100; and the Coulomb friction is 10 Newton. The lateral axis in the figure is the input displacement to the LuGre model, with a unit of micrometer. The vertical axis is the output friction in Newton. It is seen from Figure 3.1 that the stiction is bigger than the Coulomb friction. The friction rises up and quickly reaches its maximum which is called the breakaway point, and then it falls down to the Coulomb friction.

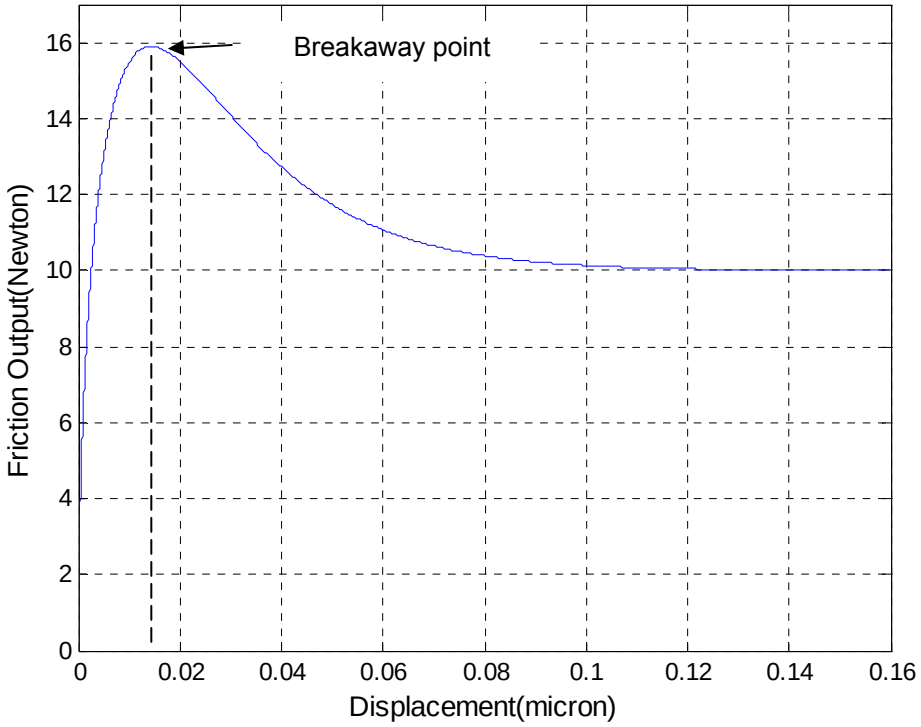

Figure 3.1 Friction vs. Displacement Simulated by Using the LuGre Model without Viscous Friction

If the viscous coefficient σ_2 equals to 25 and the damping of the tangential compliance σ_1 is 0, the friction response to the displacement is shown in Figure 3.2. As the input is parabola, the velocity increases with time. As a result, the friction force increases with the velocity increase, as seen from Figure 3.2.

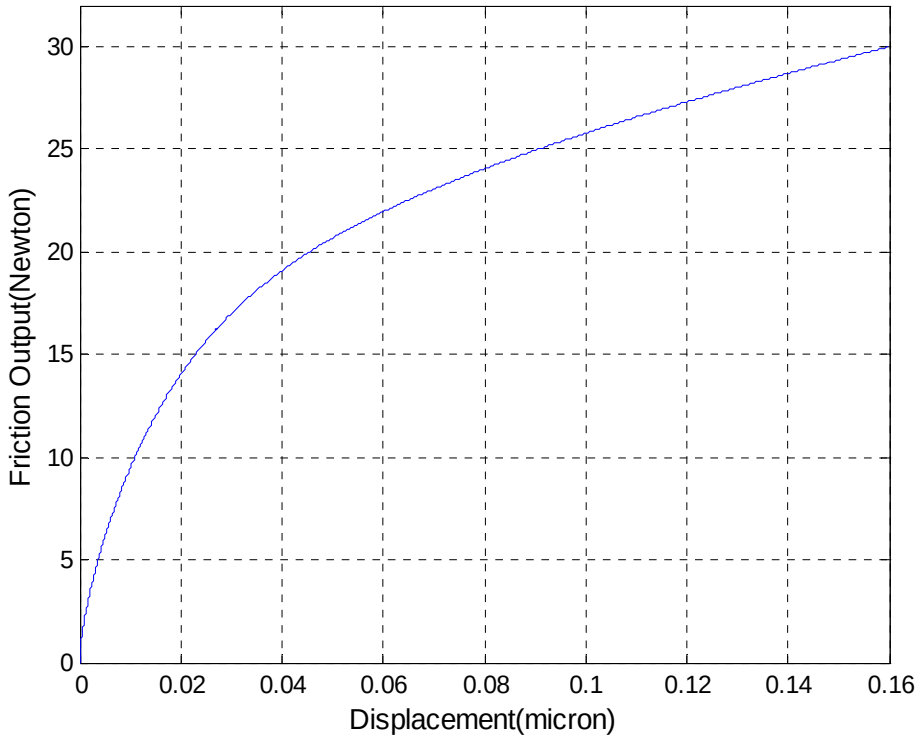

Figure 3.2 Friction vs. Displacement Simulated by Using LuGre Model without Damping of the Tangential Compliance

If both the damping coefficient of tangential compliance σ_1 and viscous coefficient σ_2 are chosen to be zero, i.e. both of the damping terms are excluded, the LuGre model becomes the Dahl model and the friction response is shown in Figure 3.3. It is seen that in the figure there is no stiction overshoot, viscous friction, Stribeck effect, and breakaway point on the curve.

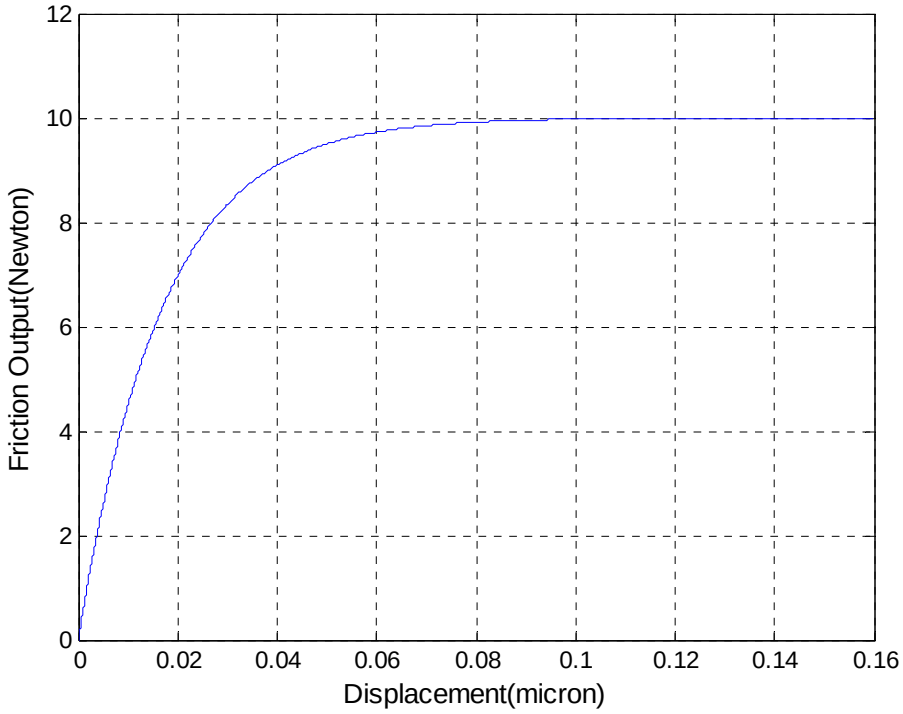

Figure 3.3 Friction vs. Displacement Simulated by Using LuGre Model without Viscous Friction and Damping of the Tangential Compliance

If both two damping terms are included, and the damping coefficient of tangential compliance σ_1 is 100 and viscous coefficient σ_2 is chosen to be 25, the stiction is greater than the one in Figure 3.1 due to the contribution from the damping of the viscous friction. The Stribect effect is seen on the curve. When the velocity increases and the object starts to slide, the friction force increases with velocity because of the viscous friction, which is shown in Figure 3.4.

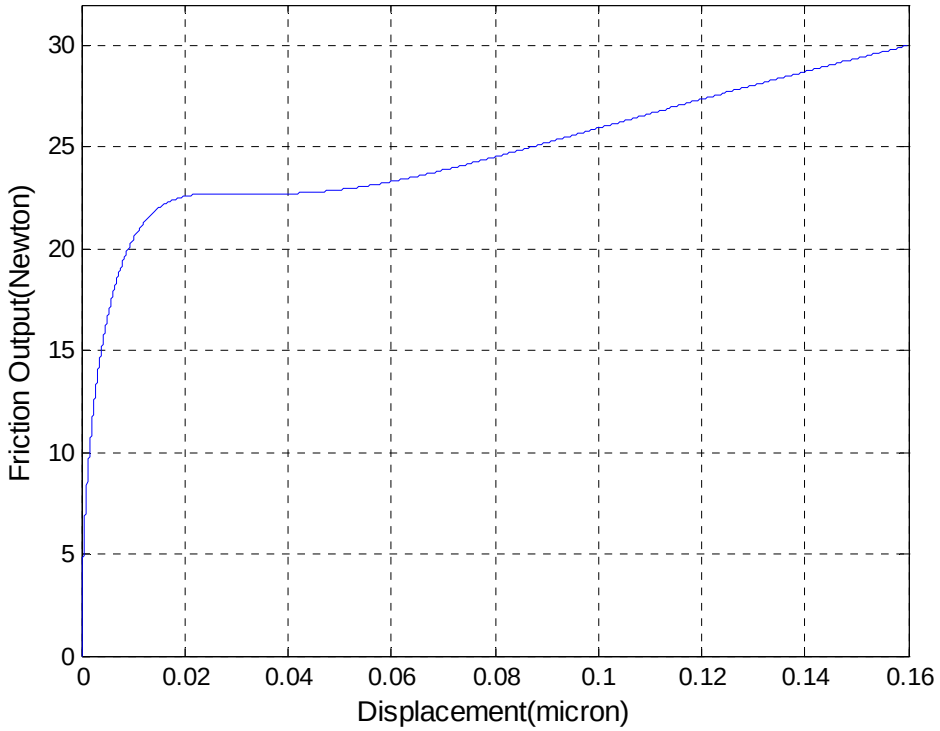

Figure 3.4 Friction vs. Displacement Simulated by Using the LuGre Model

It is seen from the above that LuGre model possess all the features of Dahl model. Furthermore, the stiction, viscous friction and Stribeck effect are included and represented by the LuGre model. Thus, the LuGre model adopted can represent the pre-sliding fiction involved in the PDSS actuator.

3.3 Modeling of the Piezoelectric Actuator and the Stage

Considering its dynamic characteristics, the PEA is modeled as a mass-spring-damping dynamic system with nonlinear components by M. Goldfarb and N. Celanovic. [Goldfarb and Celanovic,

1997] and H. J. M. T. A. Adriaens *et al*. [Adriaens *et al*., 2000] Although in the PEA studies the researchers took much effort to resolve the problem of nonlinearity, e.g. hysteresis, in most applications the PEA was treated as a linear actuator [Pohl, 1987; Chang and Li, 1999]. This linear consideration of a PEA is also found in the current IEEE standard [IEEE Standard on Piezoelectricity, 1987].

One of the reasons for linear assumption of the PEA model is that the elongation of PEA is far less than the full length elongation in our experiment. In experiment, what we interested in is not only the characteristics of the PEA under a single triangle voltage input wave, but also that of the PEA in the whole range of the PDSS actuator the saw-tooth voltage adopted as input. It is not necessary to use the maximum elongation of the PEA under maximum voltage. The PEA what we are using is AE5050D16 made by NEC/TOKIN Corp. The full length of its elongation could be 17.4 ± 2.0μm under 150volts driving voltage. In our experiments, the voltages has been applied to the PEA are less than 80 volts about half of the upper driving voltage limit. In shorter elongation range the effect of hysteresis appears less obvious.

Secondly, the dynamics of the combination of the PEA and the stage together shows linear character in experiments. The PEA is not used separately. One end of it is fixed with a stage on which the end-effecter is moving back and forth the other end is fixed on the frame, which is employed to support the PDSS actuator mechanism. In simulation, the dynamics of the PEA and the stage are being considered as a whole. It is found in our experiments that the heavier stage is used the more obvious character of second order dynamic system is shown. To explain why this could happen, we may go back to our assumption that this PEA and stage system is same as a

mass-spring-damper system, where the mass of this system equals to the combination of the PEA and the stage. If the stage is quite heavier than the PEA, the mass of the PEA would be neglected. Just like mass-spring-damper system, when the spring pushes a mass and the mass of spring is neglected. In our case, the stage is measured 98.2g; the PEA and the fixtures with it are approximate 4g, less than 4% of the whole mass. The mass-spring-damper assumption shows us the PEA in the whole mechanism could be approximated as a spring as long as the mass and the damping are considered in the whole mass-spring-damper system.

Thirdly, the sensor is not sensitive to detect tiny difference. The sensor for measuring displacement of elongation is Kaman inductive displacement sensor which has high resolution but with noise. Trying to obtain data from the sensor in data acquiring, a filter was applied to reduce the noise. In spite of the filtering, the noise is still significant. With the noise of the sensor, the hysteresis is less important for displacement measuring. And this linearity of the combination of the PEA and the stage system was also validated by the experiments that are presented later on.

In the PDSS actuator, the PEA is used to drive a stage, as shown in Figure 3.5. The combination of the PEA and the stage is modeled as a simple mass-spring-damping system, the interaction force between the PEA and the stage, denoted by F_s, is given by [Adriaens, *et al*. 2000]

$$F_s = m_s \ddot{y} + c_s \dot{y} + k_s y \tag{3.15}$$

where y represents the displacement of the stage, m_s the stage mass, c_s the stage damping coefficient, and k_s the stage stiffness. These terms are applied to the following Figure 3.5 as well, where F_p is the transformed force from the electrical side of PEA.

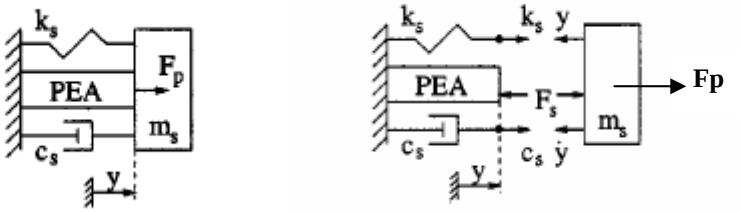

Figure 3.5 Force Analysis of the System of a PEA and a Stage [Adriaens, *et al*. 2000]

By ignoring the hysteresis effect and other nonlinearity, a combined system of a PEA and a stage is modeled as a second order system, which is given by

$$m\ddot{y} + c\dot{y} + ky = Tu \tag{3.16}$$

where u is the voltage signal applied to the PEA, and m represents the mass of the PEA and the stage, c is the damping ratio, k is stiffness, T is electrical-mechanical transformer ratio. The values of these parameters are depending on the geometries and masses of both the PEA and the stage. The relations between them are [Adriaens, *et al*. 2000]

$$m = \frac{4m_p}{\pi^2} + m_s \tag{3.17}$$

$$c = c_p + c_s \tag{3.18}$$

$$k = k_p + k_s \tag{3.19}$$

where m_p, c_p, and k_p are the mass, damping, and stiffness of the PEA respectively.

This model is adopted and used in this study and the parameter values are identified by experiment.

3.4 Development of the Piezoelectric-Driven Stick-Slip Actuator Model

In this section, a model for the piezoelectric-driven stick-slip actuator is developed by using the piezoelectric actuator (PEA) model and the presliding friction model, reviewed and examined in the preceding sections.

The schematic of a piezoelectric-driven stick-slip actuator is illustrated in Figure 3.6, along with the free body diagram showing the forces on them.

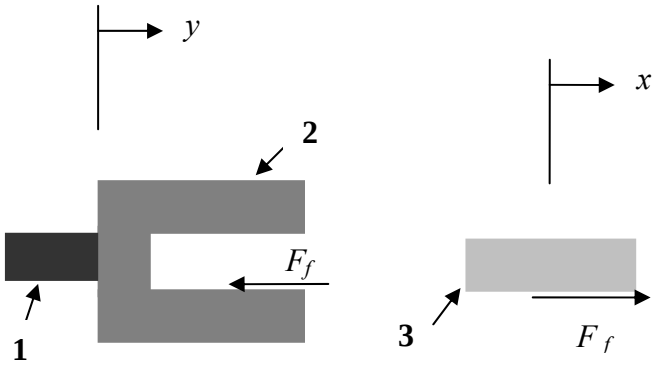

Figure 3.6 Free Body Diagram of the Piezoelectric-Driven Stick-Slip Actuator in Stick Phase

For the combination of Object 1 and Object 2, the model given in Equation (3.14) is adopted and given by in the following, if the friction force between Object 2 and Object 3 is considered,

$$m\ddot{y} + c\dot{y} + ky + F_f = Tu(t) \tag{3.20}$$

where $u(t)$ is the voltage signal applied to the PEA, F_f is the friction force, which can be represented by using the model reviewed in the preceding section. Specifically, it is given by Equation (2.15) and (2.16), i.e.

$$\dot{z} = \dot{x}\left(1 - \frac{\sigma_0}{|f_C|}\operatorname{sgn}\dot{x}\cdot z\right) \tag{3.21}$$

$$F_f = \sigma_0 \cdot z + \sigma_1 \cdot \dot{z} + \sigma_2 \cdot \dot{x} \tag{3.22}$$

For Object 3 or the end-effecter, there is only the friction force acting on it. Thus, one has

$$m_e\ddot{x}_e = F_f \tag{3.23}$$

where the displacement of the end-effecter is denoted with x_e, the mass of the end-effector is m_e. The friction force is very small comparing to force generated by the PEA, thus F_f is ignored. The second order dynamic expression becomes

$$m\ddot{y} + c\dot{y} + ky = Tu(t) \tag{3.24}$$

It is noted that $u(t)$ in Equation (3.21) can be any asymmetric waveforms to drive the end-effector, e.g. the sawtooth wave as shown in Figure 3.7. If the sawtooth voltage wave is the input into the PDSS actuator, in the period when the voltage is increasing, the force due to inertial is less than the friction, the end-effector Object 3 sticks to the stage Object 2; and when voltage begins to decrease suddenly, the inertial force is larger than the friction, resulting in slipping between the end-effecter Object 3 and the stage Object 2.

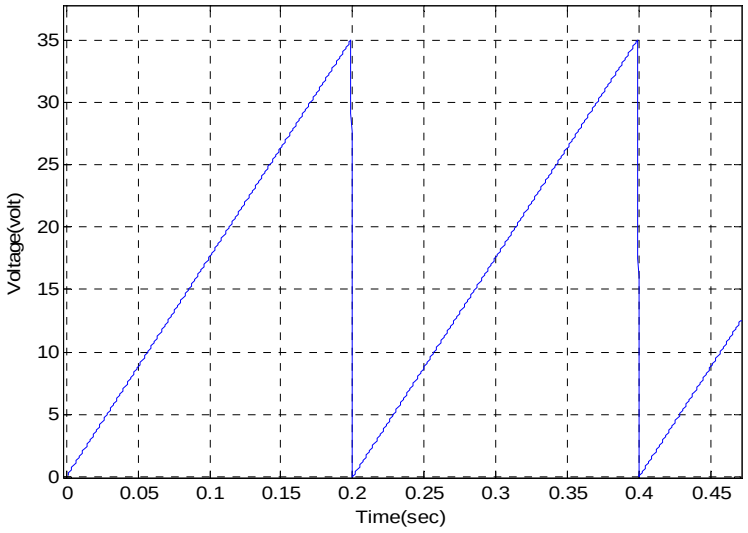

Figure 3.7 Sawtooth Voltage Input for the PDSS Actuator

The displacement output of PEA y is also the displacement of the stage. If the relative displacement between the displacement of the stage y and the displacement of the end-effecter x_e is denoted with x, the displacement x in the PDSS actuator model can be expressed as

$$x = y - x_e \tag{3.25}$$

where in the equation x_e is the displacement of the end-effecter, it is the output of the PDSS actuator, which is measured by the inductive displacement sensor in experiment. And then Equation (3.18) to (3.22) is the mathematic expressions of the developed PDSS actuator model.

As mentioned in chapter 2, the simplest form of the friction models is the Dahl model. Thus, the reasonable approach to fulfill the simulation is to employ the Dahl model as the initial attempt of the friction modeling of the PDSS actuator, and using LuGre model to do the modification and improvement. As the research going on, it was found that inducing damping terms into the Dahl model can also reduce the oscillation generated in simulation with the Dahl model and fully express the details of this process. With the damping item added into the Dahl model the friction model becomes LuGre model as following:

$$F_f = \sigma_0 z + \sigma_1 \dot{z} \tag{3.26}$$

Different to the equation (3.19), in the above expression of the LuGre model, the friction force F_f only takes one damping term into consideration, i.e. the term related to the velocity of the frictional deformation $\sigma_1 \dot{z}$. The contribution from the relative velocity $\sigma_2 \dot{x}$ between the end-effector and the stage is neglected, i.e. σ_2 is supposed to be zero.

3.5 Summary

In this chapter, different friction models were examined and compared, and the LuGre model is chosen to be used in this research to model the friction involved in the PDSS actuator. By simulation, the characteristics of LuGre model is investigated and examined. The combination of the piezoelectric actuator (PEA) and stage is modeled as a linear mass-spring-damper second order dynamic system. Finally, the development of a model to represent the displacement of the PDSS actuator is presented.

CHAPTER 4 EXPERIMENTAL SYSTEM SETUPS

4.1 Introduction

In the preceding chapter, the development of a model for the PDSS actuator is presented. To experimentally verify this model, a PDSS actuator and a sensor system for measuring displacement were prototyped and developed, which are presented in this chapter. In particular, the prototype of the PDSS actuator prototype design is discussed in § 4.2; and the development of the data acquisition and displacement measuring system in § 4.3. Included in § 4.3 is also the description of the function of the main component of the sensor system, which is followed by the calibration of the displacement sensor used in the system in § 4.4.

4.2 Prototype of the PDSS Actuator

To verify the developed model, one prototype of the PDSS actuator is designed and developed. The schematic of the PDSS actuator prototype is shown in Figure 4.1, and a picture of the prototype is given in Figure 4.2, along with the displacement sensor. The PDSS actuator prototype mainly consists of a PEA, a stage, an end-effector, a wheel, a frame, and a platform. The end-effector can slide on the stage that is driven by the PEA. Particularly, made from brass,

the end-effecter has a right triangle cross-section. The end-effector is placed on the stage with a 90 degree V-shape concave, which is made of Aluminum 6061-T6. As such, the bottom surfaces of the end-effecter contact with and are able to slide on the two concave surfaces of the stage. The contact surfaces on both the end-effecter and the stage are machined to be smooth with less than 0.37 arithmetic mean deviation of the roughness profile.

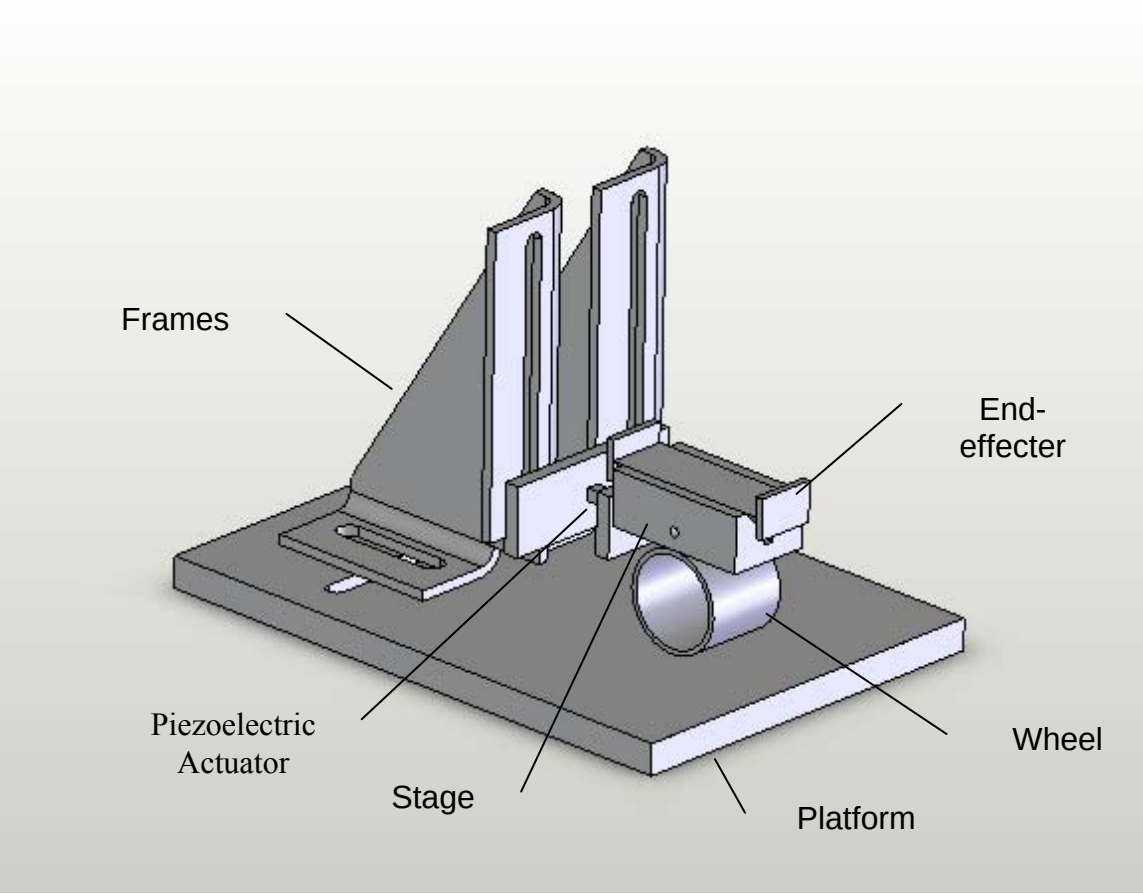

Figure 4.1 Schematic of the PDSS Actuator Prototype

The wheel is the name of an aluminum thin wall cylinder with 40 millimeter diameter, which can roll freely on the base in order to minimize the involvement of the friction between the stage and the platform. As a fact, compared to the elongation of the PEA (typically several micrometers),

the diameter of the wheel is huge, and thus the rolling of the wheel is trivial and the friction between the wheel and platform can be ignored. As a base, the platform supports the prototype, and the frames are screwed on the platform. This PDSS actuator was manufactured in Engineering Shop in College of Engineering in University of Saskatchewan.

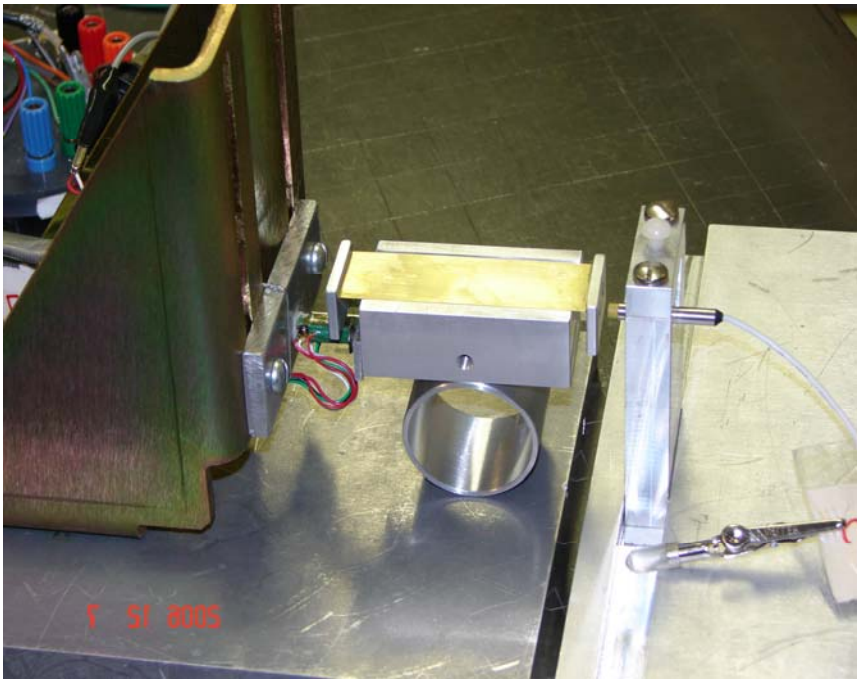

Figure 4.2 Picture of the PDSS Actuator Prototype

The piezoelectric actuator (PEA) selected for the prototype is a resin coated Tokin AE0505D16 (made by NEC/TOKIN Corp.) with a size of $5 \times 5 \times 20$ mm^3 and a density of 8×10^{-3} g /mm^3, which is driven by ENV400/ENT400 (made by Piezosystem Jena Inc.). The elongation or the displacement of the PEA is measured by the strain gauge mounted on the PEA. A 9-pin connector is used to connect the strain gauge output wires from the PEA and driving voltage

input wires to the PEA. The maximum elongation of the PEA is 17.6 ± 2 μm under 150 volts driving input without load.

4.3 Data Acquisition and Displacement Measuring System

4.3.1 System Overview

The experimental system developed in this research for the model verification has two functions: one function is to generate the voltage signal applied to the PEA, and the other one is to measure the displacement of interest in this research. An overview of this system is shown in Figure 4.3 schematically, which consists of a custom-made dSPACE & Simulink computer control system, a DS1102 controller board, piezoelectric actuator amplifiers, the PDSS actuator including the piezoelectric actuator, strain gauges and a signal conditioner, and an inductive displacement sensor system.

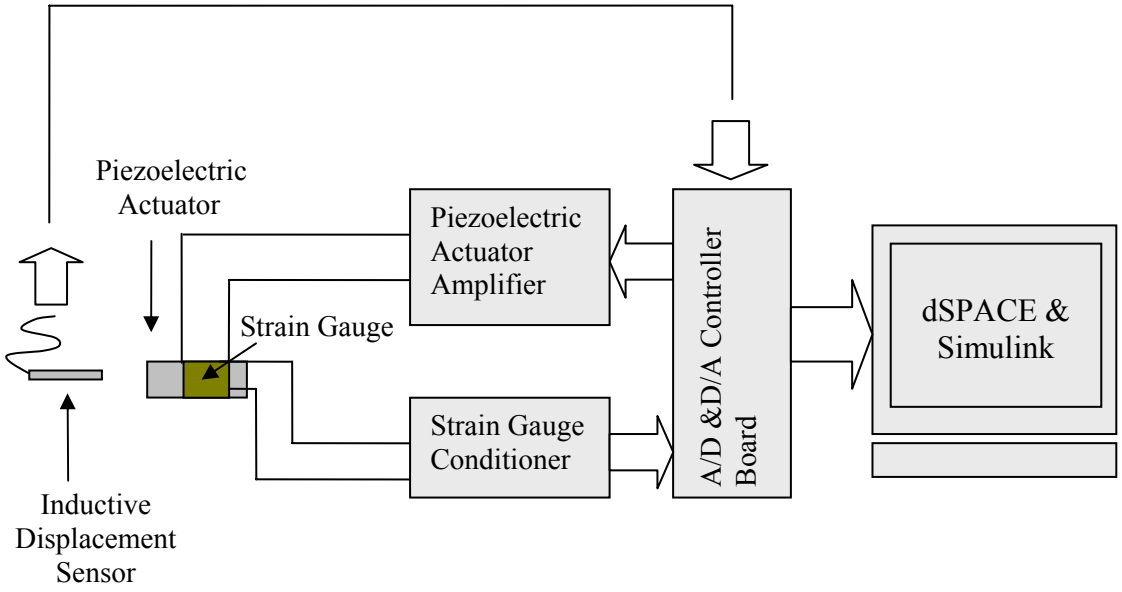

Figure 4.3 Overview of the Data Acquisition and Displacement Measuring System

The digital signal applied to the PEA is generated in the dSPACE & Simulink computer control system, which was developed in the ControlDesk of dSPACE. The ControlDesk is the experiment software used to control, monitor, and facilitate real-time experiments. It allows users to load experiment hardware in virtual space in dSPACE. Employing a variety of virtual instruments offered in the Instrument Kits, users can build virtual instrument panel to handle and monitor experiment via a user interface. The experiment process is triggered in the ControlDesk of dSPACE, which is then regulated by the processor on the DS1102 controller board. The generated signal is then fed to the D/A converter on the DS1102 controller board, where the digital signal is converted to analogous voltage signal. This signal is then amplified by the amplifier and used to drive the PEA. Two kinds of sensor are used to detect the displacement: one is the strain gauges and the other one is the inductive displacement sensor. The electrical signal of the elongation of the PEA detected by the strain gauge is adjusted and amplified by the

strain gauge conditioner, and then sent to the A/D converter on the controller board. On the other hand, the electrical signal of the displacement change detected by the inductive sensor is sent straightly to the A/D converter on the controller board. Both of the electrical signals from the sensors on the A/D converters are acquired by the ControlDesk of dSPACE. These obtained data of displacement change are displayed in graph and in digital numbers on the virtual panel of ControlDesk, and restored for further analysis.

4.3.2 Main Components of the Hardware System

Following the overview of the experiment system in the previous section, this section presents details of the main hardware components used in the experiment system. The center of this experiment system is the dSPACE & Simulink computer control system. It is known that Matlab is a high-performance language for technical computing and Simulink is one of its powerful tools and specifically used for modeling, simulating, and analyzing dynamic systems. Also, it is known that dSPACE is primarily designed for rapidly prototyping of control system. dSPACE works as an interface between Simulink and real-time hardware and instruments. Through its controller board, the blocks of Simulink diagram are connected to the outside real-time hardware. By communicating with outside hardware, it can either acquire experiment data from real system or apply designed control strategy to real-time system.

Built with a Texas Instruments TMS320C31 floating-point digital signal processor (DSP), the DS1102 Controller Board is the control device between ControlDesk of dSPACE and the real-

time hardware. It is designed for the development of high-speed multivariable digital controllers and real-time simulation [dSPACE digital signal processing and control engineering GmbH]. The special designed DS1102 Controller Board has 4 units of 12 bit and 16 bit A/D converters and 4 units of 12 bit D/A converters, i.e. each unit A/D or D/A has 12 or 16 binary digital ports. The two types of ADCs are:

- Two 16 bit 250 KHz sampling frequency A/D converters with integrated sampling holds, which keep the sampling signal waiting for the processor to collect data.
- Two 12 bit 800 KHz sampling frequency A/D converters with integrated sampling holds.

The 16 bit 250KHz A/D converter has higher precision and longer sampling period compared to the 12 bit 800KHz A/D converter. The ADCs have a range of ±10V for input voltage [dSPACE digital signal processing and control engineering GmbH]. In this research, since the displacement is small, the high precision 16 bit A/D converter was chosen for the output of inductive displacement sensor. Since there is only one output from the controller board, one of the four D/A 12 bit converters is employed.

The piezoelectric ceramics actuator amplifier set has 3 units of ENT 400 amplifier with 2 units of Jena-ENV 400 power supplier. It has 60 watts power supply and is able to provide the PEA with a very fast position response. In this research, only one amplifier was used to drive the PEA, and the amplifier has a gain of about 15, which is connected to the DS1102 controller board D/A converters. Since D/A converter has a gain of 10, the total amplification gain to the PEA is about 150, i.e. if 1 volt voltage is set and output from dSPACE, then the voltage applied on PEA will be around 150 volts. In experiment, if 50 volts is needed to be applied on PEA, the actual input

voltage generated in the ControlDesk will be about 0.312 volts. The one to one corresponding relationship test has been conducted, and the result is shown in the table given in Appendix 3.

Two pieces of the strain gauge are glued on each of the two opposite sides of PEA to measure the longitudinal elongation. The individually designed strain gauge conditioner is Vishay 2120B Conditioner Module and Vishay 2110 Power Supply Module. The outputs of the strain gauge conditioner are fed to the A/D converters of the DS1102 controller board. The strain gauges and the strain gauge conditioners were calibrated in other research, and the following translating equation was obtained to relate the conditioner output voltage to the elongation of the PEA used in this research.

$$PZT3 - L1 = (ADC\#\,Input + 0.0853) \times (-22.08) \tag{4.1}$$

where *ADC#1Input* is the ADC input voltage, *PZT3* is the elongation of the PEA, and $L1$ is the length of the PEA before elongation.

The other type sensor used for the displacement measuring in this research is the inductive sensor, which is made by Kaman Instrumentation Corporation. This sensor needs an independent electrical power supply which provide up to 18 volts voltage or to 1.5 amps current to the sensors. The resolution of the sensor is 1 angstrom. The output voltage range of the Kaman inductive sensor is 0 to 10 volts. Since the input voltage range of the ADC of DS1102 controller board is from – 10 volts to 10 volts, the output of the sensor is acceptable for the controller board.

4.3.3 Simulink Models Used in the Experimental System

The development of the experiment system software is briefly discussed in this section. At first, a Simulink model is created to describe the input signal, control unit, output signal, and hardware I/O device. This Simulink model is then transformed into the program of the codes of dSPACE and downloaded onto the processor on the DS1102 controller board by applying the Real Time Workshop (RTW) of Matlab and Real Time Interface (RTI) of dSPACE. Finally, the user can run the program to operate the created experiment system.

Simulink of Matlab was employed in the model construction and the algorithm implementation. The Simulink model of the experiment system is given in Appendix 2. To access the real-time hardware through dSPACE from the Simulink model, dSPACE provides a specific Real-Time Interface, i.e. the RTI1102 library [dSPACE GmbH, 1999] which contains dSPACE blocks describing I/O hardware of the controller board. Using the Input/Output blocks in RTI 1102 library, the Simulink blocks are connected to the I/O interface of DS1102. After the model has been created in Simulink, the model will be transformed into real-time code which can be read by the Real Time Interface of dSPACE. The Real Time Workshop in Simulink performs the transforming work. The Real-Time Workshop is a product of MathWorks Inc., which can produces programming codes directly from Simulink model and automatically build programs to realize real-time application. Via the Real-time Workshop, one may run a Simulink model on a remote processor and interact with other hardware to conduct real-time control operation [Real-Time Workshop, MathWorks, Inc.]. The Real-Time Workshop invokes the Target Language Compiler (TLC) to transform a Simulink model into an intermediate description saved in ASCII code form. Then the Target Language Compiler translates the intermediate description stored in

language-independent form into the target specific codes which can be executed in different environments, e.g. Real-Time Interface (RTI) of dSPACE [Real-Time Workshop, MathWorks, Inc.]. In dSPACE, the main component for doing this translation is also Real-Time Interface (RTI). Applying the Build process in Simulink, the Real Time Workshop translates the description of Simulink model into the codes executable for RTI and downloads these codes onto the processor on the controller board. These codes not only have the executable description of the block of the Simulink model, but also contain the information such as the parameter values, sampling time, vector length, and etc.

The Simulink model of the experiment system of the friction model determination, which is in Appendix 2, is similar as the one in second parameter identification experiment, except the step input is replaced by the sawtooth & reverse sawtooth wave generator which is seen on the upper-left corner of the figure in Appendix 2. Different to the forward saw-tooth wave, the reverse sawtooth voltage wave makes the PEA to contract first and then extend, and the stage still does the reciprocating motion and the end-effecter is driven to do the inertia sliding movement but in opposite direction. This reverse sawtooth wave drives the end-effecter back to initial position after the forward motion such that the next forward motion may start from almost same zero point.

4.3.4 Experiment File Setup of ControlDesk

Once the experiment model is created in Simulink and transferred into dSPACE codes downloaded to the processor on DS1102 controller board, the next step is setting up experiment files in the ControlDesk of dSPACE which is specifically designed for the current experiment managing, controlling, monitoring, and automating experiments. The experiment files design also includes the virtual instrumental panel design, which includes connecting the variables of the Simulink model to the variables on the virtual instrumental panel, as well as determining data acquisition settings and other setting of PDSS actuator experiment. dSPACE applies system control by the ControlDesk which can control and monitor the real-time experiment, manage the hardware of dSPACE, construct virtual panel using virtual instruments, and capture the experiment data by configuring the data acquisition instruments and data capturing process.

The ControlDesk's Data acquisition instruments make all the experiment data running in the experiment hardware accessible and could be transmitted to other system for data analysis [ControlDesk Experiment Guide, dSPACE GmbH 1999]. The ControlDesk can manage experiments by choosing various type files which are needed to form a general experiment file. In the ControlDesk, the experiment file is the basis for all further actions. The dSPACE's experiment file is one file linked to all files associated with an experiment [ControlDesk Experiment Guide, dSPACE GmbH 1999]. For instance, a LAY file is a layout file with the information about instrument kind, size, position, and attributes of the instrument which is used in the instrument panel layout. MAT file is MATLAB binary files recording reference data

acquisition. An OBJ file is an object file executable for the real-time processor on the controller board DS1002.

This experiment file was built from the Simulink model and the generated OBJ object file was downloaded to the processor on DS1102 controller board. Included in the PDSS actuator experiment file the virtual control panel file was constructed by using the ControlDesk's Instrument Kits. The same virtual control panel is applied to manage all the experiments and to monitor the experimental processes but display the different variables. This control panel consists of following devices: a Plotter, a Numericinput, two output Displays, as shown in Figure 4.6. In the parameter identification of the friction model experiment, the Plotter shows on the same screen (1) the stage displacement acquired by the Kaman inductive sensor, (2) the piezoelectric actuator elongation acquired by strain gauge, and (3) input signal generated in ControlDesk. One Numericinput is used to input desired step voltage value. In the contrast, in the experiment of the parameter identification of the second order system experiment, the Plotter displays on the same screen (1) the displacement of the end-effecter acquired by Kaman inductive sensor; (2) the PEA displacement acquired by strain gauge, and (3) the input signal generated in ControlDesk. One Numericinput is used to show the sawtooth voltage generated in ControlDesk. Second one is connected to the variable Gain 7 of the sawtooth wave input generator to determine the voltage magnitude of the sawtooth wave. The third Numericinput is connected to the variable Gain 14 of the generator to determine the voltage magnitude of the reverse sawtooth wave. The Two Displays show the output displacements of the strain gauge and the inductive displacement sensor individually. Then each of the three signals displayed graphically and digitally simultaneously.

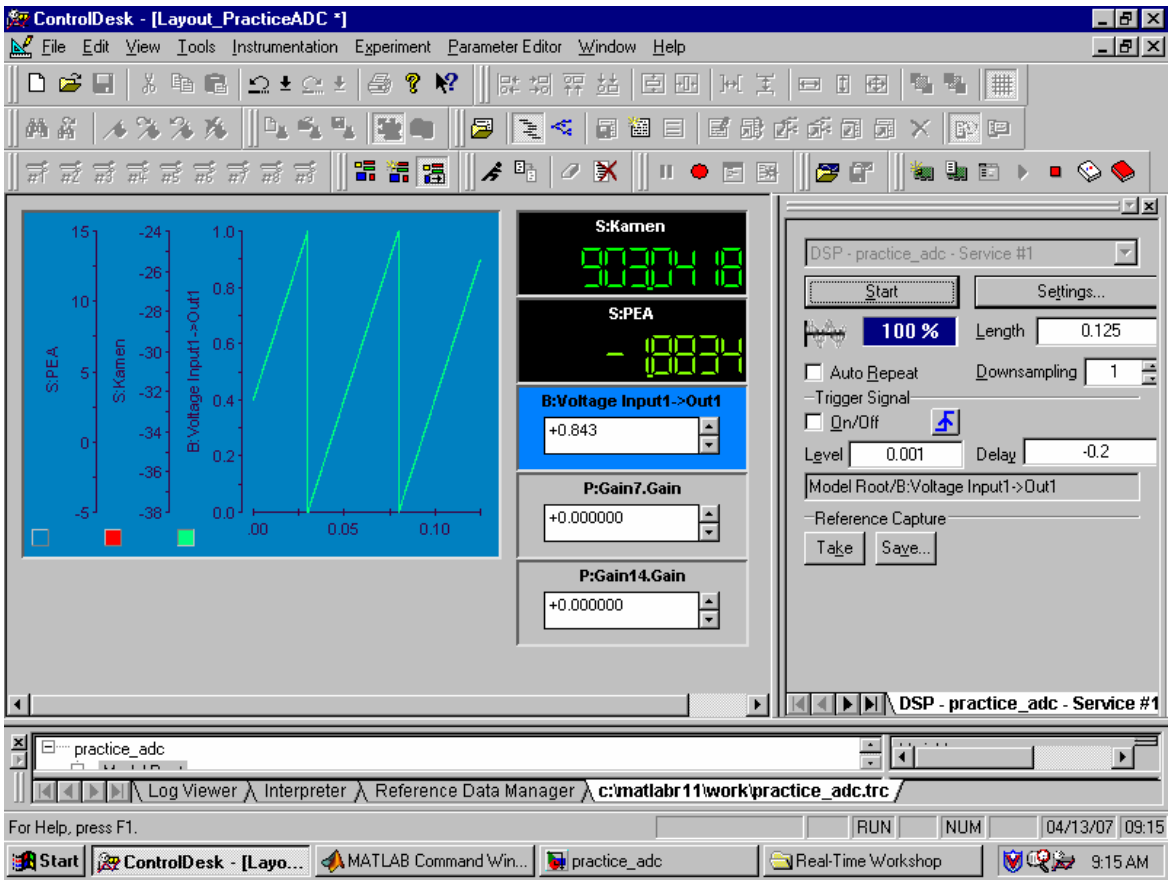

Figure 4.4 Virtual Control Panel of the PDSS Actuator Experiment

For convenient, the Capture Settings Window and the Tool Window is displayed on the right side of the control panel. The Capture Settings Window is employed for the experimental setting-up, e.g. defining the time period of a single experiment, the sampling time, and the number of automatically repeated experiments, the trigger signal, the length of the time delay, and the data acquiring and data storing. Also, there are start and stop buttons on the Capturing Setting window. The percentage progress shows the percentage of the experiment that has been run. For different experiments of the PDSS actuator, the data capturing setting is different. Usually, the time delay is chosen to be 0.2 second, the sampling time is as short as possible, the

trigger signal is the input signal to the PEA, which is also the output out of the DAC on the controller board. In the Log Viewer window of the tool window at the bottom of the panel, one may observe the dSPACE's operation in prompt. The Variable Manager is employed for managing the experimental data, which includes the data display on the virtual instruments and specifying the trigger of the data acquisition process.

4.4 Sensors and Sensor Calibration

4.4.1 Sensors

In this research, a critical part of the experiments is the displacement measurement. As mentioned previously, there are two types of displacement sensor: one sensor is the strain gauge and the other one is the Kaman inductive displacement sensor. It was found by experiments that the dynamic response of the Kaman inductive displacement sensor is better than the stain gauge. Thus, the inductive displacement sensor was primarily employed for the displacement measurements, while the stain gauge was used for comparison to verify the inductive displacement sensor's output. In this experiment the inductive displacement sensor was calibrated for the purpose of dynamic displacement measuring of the PDSS actuator.

The strain gauges are used to measure the elongation of piezoelectric actuator (PEA). The strain is a measurement of deformation of an object under the action of force, which is usually defined as fractional change in full length of a material, i.e.

$$\varepsilon = \Delta L / L \tag{4.2}$$

where ΔL is the deformation or the change in length and L is the full length of the object.

To measure the strain, the most popular approach is the use of the strain gauge to convert the mechanical deformation to the electrical signal. The strain gauge is made of the electrical resistive material, which resistance varies proportionally to the strain of the material. For a strain gauge made of narrow or thin resistive wire, when it is extended a slightly longer, the wire's cross-section is reduced and its resistance is increased. Its resistance increasing is proportional to the strain increasing. It is noted that the strain gauge resistance is also affected by temperature. As a result, the temperature compensation circuit is usually used in the strain gauge devices.

The other sensor is Kaman inductive displacement sensor SMU-9000 made by Kaman Instrumentation. The inductive displacement sensor is applied to measure the displacements of both stage and end-effecter of the PDSS actuator in experiment. In this research, the inductive displacement sensor is connected to the experimental system presented previously, and the sensor has to be calibrated. In the following, the information related to the sensor, such as its working principle and output, is presented, which is followed by the sensor calibration.

The inductive sensor utilizes the inductive current technology to measure displacement without contacting the target, and has high resolution, high performance-to-price ratio, simple operation, and low power consumption [SMU-9000 User Manual, Kaman Instrumentation Corporation]. The inductive current technology is illustrated in Figure 4.5, where the measuring system consists of conductive target, sensor, cable, and electronic device. The sensor is built with coil.

The electronic device has two functions: the oscillator circuit generates pulsating signal to the coil of sensor, and the amplification circuit converts the signal into a standard measurable voltage output [SMU-9000 User Manual, Kaman Instrumentation Corporation]. In operation, an impulsive current is generated in the electronics' oscillator. Then the AC current goes through the cable to the coil. The AC current causes the electromagnetic field of one winding adding to the field of another winding. As a result, the pulsating electromagnetic field is around the coil. If the coil of the sensor is placed close to a conductive target, an eddy current is induced on the surface of conductive target. The induced eddy current in turn produces a secondary electromagnetic field which opposes and reduces the intensity of the original electromagnetic field. The gap between the coil of the sensor and the target determines the strength of the electromagnetic field. In other words, the displacement between sensor and target changes the output to the electronics. Then the electronics converts the received electrical signal into displacement.

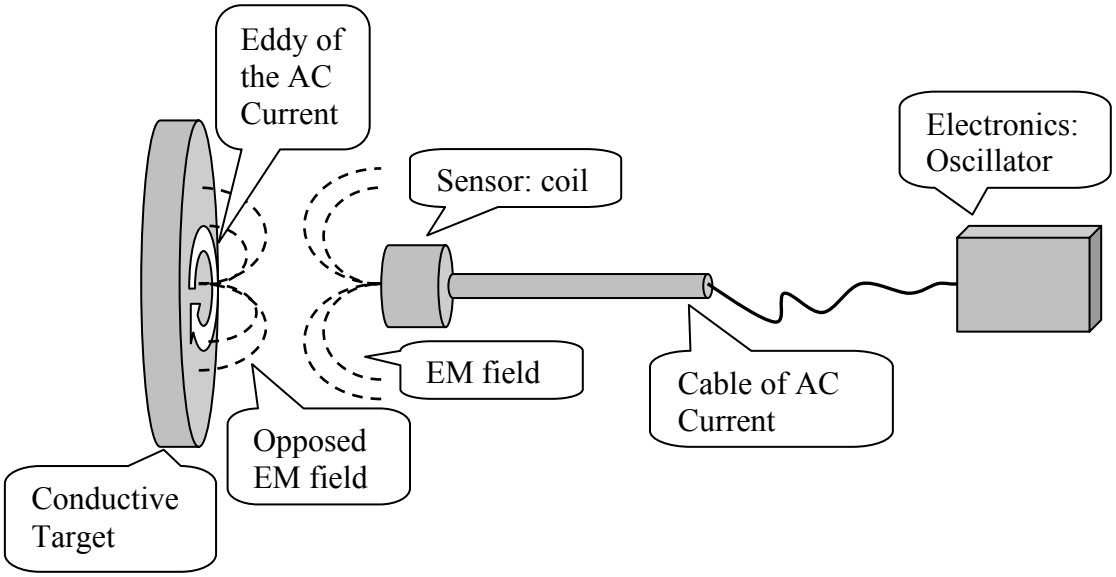

Figure 4.5 Inductive Technology [Kaman Instrumentation Corporation]

It is noted that, for the inductive sensor, there are several factors affecting the measuring. At first, the material of the target must be made of highly conductive and uniform electric property metal, such as aluminum and copper, since the resistance and permeability affects the performance of inductive displacement measuring. Since the SUM-9000 inductive sensor was calibrated by manufacturer using aluminum as the target, the target is preferred to be made of aluminum. In the PDSS prototype, given that the end-effecter was made of copper, two aluminum plates were attached to the two ends of the end-effecter. Secondly, although there is no specific requirement about the roughness of the target surface, its area should be at least 2.5-3 times the area of the unshielded sensor. In experiment, this requirement is followed. The shape of the target surface is not very restricted.

4.4.2 Sensor Calibration

Before putting it into use, the inductive sensor should be calibrated to make sure the sensor's accuracy and linearity in displacement measuring. There is a manufacturer calibration table provided by Kaman Instrumentation Corporation, for users to convert the output voltage of the sensor to the displacement. The calibration table and the regression formulae are given in Appendix 1. In this table, x denotes the voltage measured by the inductive sensor and y the displacement. Using the provided five order polynomial modification, the error of the measured displacement can be controlled less than 6 micrometers; and using the provided three order polynomial modification, the error can be less than 15 micrometers. The displacement of the sensor is in a range of 1 mm.

If the dynamics of the displacement is not concerned, the simplest way for the displacement measurement is to connect the output of the inductive sensor device to a digital voltmeter, and then to convert the voltage displayed on the voltmeter to corresponding displacement by using the five or three order polynomial formula in Appendix 1. If the dynamics of the displacement is concerned, the Simulink & dSPACE experiment system described in previous sections needs to be applied. In particular, the voltage signal from the displacement sensor was sampled and the acquired data were sent to Matlab for analysis. To convert the voltage to the displacement, the manufacturer's calibration results needs to be integrated into the displacement measuring system, i.e. using the five order polynomial calibration formula in the Simulink model of the PDSS actuator, which is shown in Appendix 2.

In the experiments, it was found the error by means of the manufacturer's calibration results is significant, which suggests a new calibration be needed. Figure 4.6 shows the setting-up for the new calibration, in which a micrometer caliper was employed to provide the known displacement. A five order polynomial was also used to correlate the measured voltage to the displacement; and the coefficients were determined based on the known displacements and the measured voltages. The five order polynomial with the determined coefficients is given as follows.

$$y_C = 3.58E-13 \cdot x_C^{\,5} - 8.69E-10 \cdot x_C^{\,4} + 7.40E-07 \cdot x_C^{\,3} - 0.0002691 \cdot x_C^{\,2} + 1.0222 \cdot x_C + 0.30871 \quad (4.3)$$

where x_C is the sensor displacement output before the calibration, and y_C is the output after calibration. The above equation was then used in the Simulink model of the PDSS actuator experiment system for measurements, which is given in Appendix 2. In addition, in order to reduce the influence of noise on the measurements, a digital filter is used and added to the Simulink model. The filter is a Digital IIR Filter provided in the Simulink library. Once the filter is put into the displacement measuring system, the noise has been reduced and the accuracy has been improved. Table 4.1 shows the calibration result at the starting and the ending points in the measuring range, in which there is a 50 μm offset. It is seen that the error of the displacement measured in the full range is less than 6 μm.

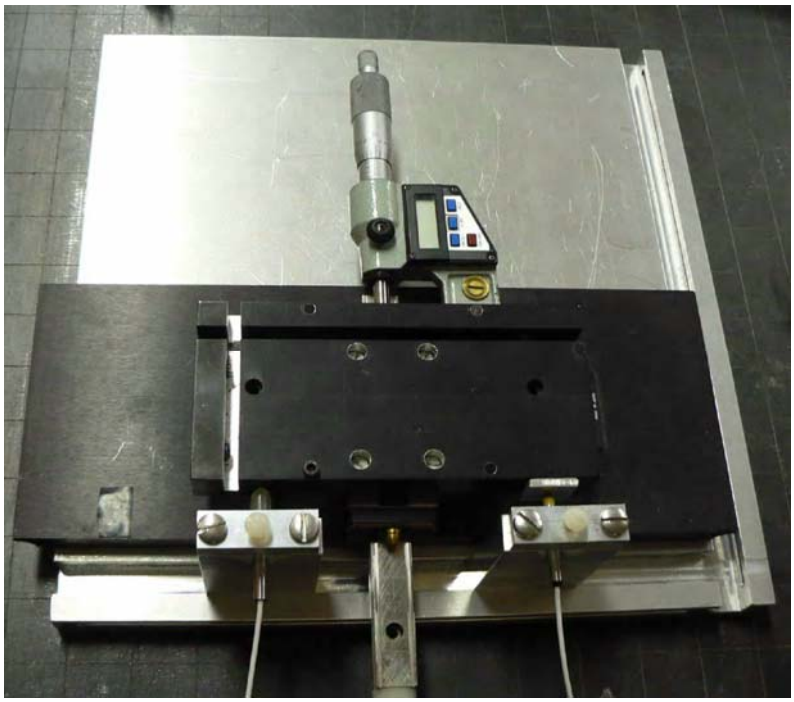

Figure 4.6 Inductive Sensor Calibration Setup

Table 4.1 Inductive Sensor Calibration (micron)

	Starting	Ending
Micrometer Caliper	0	950
Inductive Sensor (1)	- 50.1	904.4
Inductive Sensor (2)	- 49.7	905.8

4.5 Summary

In this chapter, the setup of the PDSS actuator experiment system is discussed. At first, the prototype design of the PDSS actuator is presented. Secondly, the data acquisition and displacement measuring experiment system are put forward. Finally, the sensors used in displacement measuring are discussed, which is followed by the calibration of the inductive sensor.

CHAPTER 5 EXPERIMENTAL VERIFICATION

5.1 Introduction

In the Chapter 3 and Chapter 4, the PDSS actuator model was developed and the experimental system for the model verification has been discussed. This chapter focuses on the experimental verification of the PDSS actuator model as well as the identification of the parameters involved in this model. For the parameter identification, two experiments were designed and carried out: one experiment is for the determination of the parameters of the second order system for the dynamics of the combination of the piezoelectric actuator (PEA) and the stage, and the other one is to determinate the parameters of the friction model in the PDSS actuator model. These two experiments are discussed in § 5.2 and § 5.3, respectively. In § 5.4, the experiment results are examined to illustrate the effectiveness of the developed model, which is followed by the summary in § 5.5.

5.2 Parameters Identification for the PEA and Stage Model

5.2.1 Experimental Setup

As discussed in Chapter 3, the dynamics of the combination of the PEA and the stage can be represented by using a second order dynamic system, i.e. the Equation (3.14). The parameters involved in the model were identified in this research by conducting experiments on the experimental system presented in the preceding chapter. The Simulink model created for these experiments is provided in Appendix 4. The only difference between this model and the one given in Appendix 2 (discussed in the preceding Chapter) is that the input to DS1102 DAC, i.e. the sawtooth generator input blocks are replaced by a step input block. The Simulink model was downloaded to the processor of the DS1102 controller board, such that this configuration change was applied to the ControlDesk in the dSPACE. The data of the measured displacements were taken and restored by in the ControlDesk for analysis. The description of the experimental condition is provided as follows.

1. The experiments were all conducted at the room temperature, by using the data acquisition system and displacement measuring system presented previously.
2. The step response of the combination of the PEA and stage was examined, and the parameters of its model were then identified.
3. The displacement of the stage was measured by the Kaman inductive displacement sensor, while the displacement of the PEA was monitored by using the strain gauge so as to confirm the result from the inductive displacement sensor.

4. The moving part of the prototype driven by PEA is the stage, the end-effector with one metal block, which is fixed on the stage and can not slide on the stage.

For the data acquisition in the ControlDesk, the following settings were applied.

1. The experiment length was set to be 0.5 second; and the sampling interval for data acquisition is 0.2 ms.
2. The step voltage applied to the PEA was set to be 60, 70, and 80 volts, respectively. The experiment process is triggered by the step signal so that the experiment starts after the ControlDesk detects this signal.
3. Compared to the step input to the PEA, the recorded data has a time delay of 0.2 second. This configuration was made for that the data acquiring starts 0.2 second earlier before the trigger signal comes. It makes better display of the experimental data that the signal before zero instant can be shown, and it offers the data prior to the 0 second, i.e. before the experimental process starting instant.

5.2.2 Parameters Identification

For a second order system, the dynamics can be represented by the following transfer function

$$\frac{Y(s)}{U(s)} = G(s) \tag{5.1}$$

and

$$G(s) = \frac{C\omega_n{}^2}{s^2 + 2\zeta\omega_n s + \omega_n{}^2} \tag{5.2}$$

In the time domain, the above relation can be rewritten as

$$\ddot{y} + 2\varsigma\omega_n \dot{y} + \omega_n{}^2 y = C\omega_n{}^2 u \tag{5.3}$$

In the above equations, ω_n is the natural frequency, ζ is the damping ratio, and C is the steady state gain. The values of these parameters are dependent on the physical system considered, and can be determined or identified by using either theoretical or experimental method. In this research, these values were identified by experiments for the dynamics of the combination of the PEA and the stage.

As discussed in Chapter 3, the dynamics of the combination of the PEA and stage is given by

$$m\ddot{y} + c\dot{y} + ky = Tu \tag{5.4}$$

Divided both sides of the above equation by *m*, i.e., the total mass of the PEA and stage, it becomes

$$\ddot{y} + \frac{c}{m}\dot{y} + \frac{k}{m}y = \frac{T}{m}u \tag{5.5}$$

or

$$\ddot{y} + c_m \dot{y} + k_m y = T_m u \tag{5.6}$$

where $c_m = \frac{c}{m}, k_m = \frac{k}{m}$, $T_m = \frac{T}{m}$. The second order system of the combination of the PEA and stage can be determined, as long as the parameters c_m, k_m, and T_m are found. The equation (5.6) has the same form with equation (5.3), so that the model can be determined if ζ, ω_n and k are found. For the identification of the values of these parameters, the step responses of the combination of the PEA and the stage were measured by using the inductive sensor, in which the voltage input of 60, 70, and 80 volts were applied to the PEA, respectively. The measured responses are shown in solid lines in Figure 5.1. It can be seen that the step responses show the characteristics of a second order system.

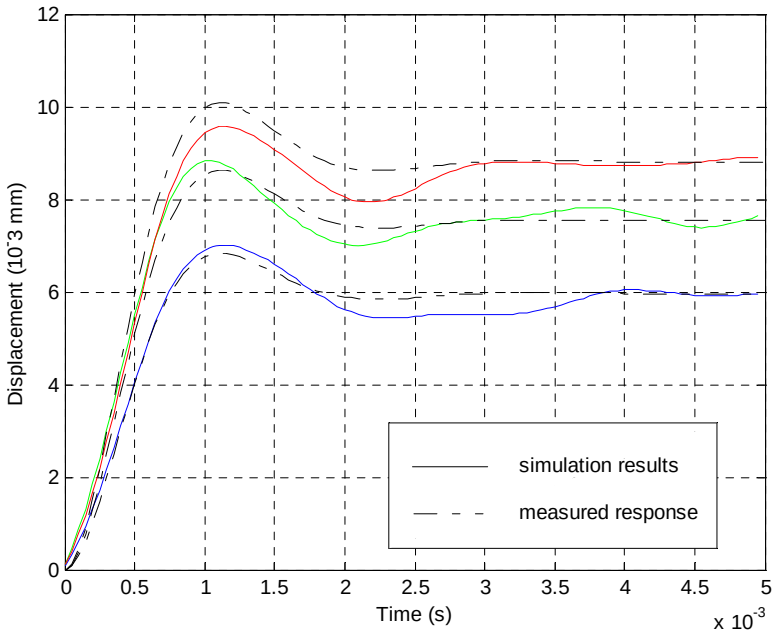

Figure 5.1 Simulated and Measured Step Responses of the Combination of the PEA and Stage

A straightforward approach to identify the second order system parameters is based on the measured transient responses, specifically the rising time T_r, settling time T_s, peak time T_p, and overshoot *OS%* of the step response. From Figure 5.1, the values of T_P and $OS\%$ can be easily determined. Thus, the damping ratio ζ and the natural frequency ω_n can be evaluated. Once the step response reaches its steady state value, the steady state gain T_m becomes the ratio of the generated force of the PEA to the input voltage. Therefore, the parameters of the second order system of the PEA and the stage can be determined, which is obtained as follows.

As T_P and *OS%* are known, the damping ratio ζ and the natural frequency ω_n of a second order system can be individually calculated in following equations.

$$\zeta = \frac{-\ln\left(\%OS \times 100\right)}{\sqrt{\pi^2 + \left(\ln^2 \%OS \times 100\right)}} \tag{5.7}$$

$$\omega_n = \frac{\pi}{T_p\sqrt{1-\zeta^2}} \tag{5.8}$$

Based on the above relations, the Matlab program for the parameters identification was developed, which is provided in Appendix 7 "Matlab Program for Second Order System Parameters Identification". In this program, the experiment data acquired by the dSPACE data acquisition system are used; and the damping ratio ζ and the natural frequency ω_n are calculated for 60 volts, 70 volts, and 80 volts experiment individually. The average of above three data is taken as the final value of ζ and ω_n. By doing so, the values of ζ and ω_n were found to be 0.524

and 3303.1 rad/sec. Thus, the values of the parameter in Equation (5.6) were then obtained, which are given by

$$c_m = 0.0035 \ kg/s$$

$$k_m = 10.9098 \ kg/s^2$$

In the steady state, the relationship between the input and the output relation is

$$k_m \cdot y_{ss} = T_m \cdot u_{ss} \tag{5.10}$$

u_{ss} is the given input voltage and y_{ss} is the steady state displacement measured by inductive sensor. T_m was calculated from the measured displacement and given by $T_m = 1.1532 \ N/v$.

The identified parameters of the second order system model are used to simulate the step response of the combination of the PEA and the stage. The simulated results are shown in Figure 5.1 in dash lines, along with the measured results in solid lines. It can be seen that the simulated results are in the close agreement with the measured ones, and the calculated coefficient of determination r^2 is 0.9708 for the developed second order system model.

In the above identification experiment, the inductive sensor was observed to have a time delay, approximated in a range of 0.6 ms ~ 1.0 ms. To eliminate its influence, the data were shifted in terms of the time delay for the data analysis. In addition, it is also noticed that, if the voltage applied to the piezoelectric actuator is less than 50 volt, the noise overwhelms the overshoot of

the step response. Thus, the voltage inputs were chosen as 60, 70, and 80 volts, respectively, in the experiments.

5.3 Parameters Identification for the Friction Model

To determine the parameters involved in the friction model, experiments were designed and conducted, which are detailed as follows.

1. All the experiments were conducted at the room temperature.
2. The displacement of the end-effecter was measured by using the Kaman inductive displacement sensor, and the strain gauge was used to show the motion of the PEA and the stage of the PDSS actuator under the sawtooth wave input.
3. The end-effector with a metal block attached can freely slide on the stage that was driven by the PEA.

For the data acquisition, the following settings were applied.

1. The sampling interval was set 1 ms for the input with a frequency of 5 Hz, and 0.25 ms with a frequency of 20 Hz.
2. The trigger signal is the sawtooth wave.
3. The experiment length was set 10 seconds for the 5 Hz experiment and 2.5 seconds for the 20 Hz experiment.
4. The Time Delay is - 0.2 second, i.e. the data acquisition process starts 0.2 second prior to the trigger signal of the sawtooth input comes.
5. The magnitude of the sawtooth wave applied to the piezoelectric actuator set 35, 55, 65, and 75 volts, respectively.

Part of the displacements measured in the experiments are given in Figure 5.2 in a dark solid curve, which are the measured displacements as the sawtooth voltage with a magnitude of 65 volts and a frequency of 5 Hz was applied to the actuator. These measured displacements were used to determine the parameters of the friction model.

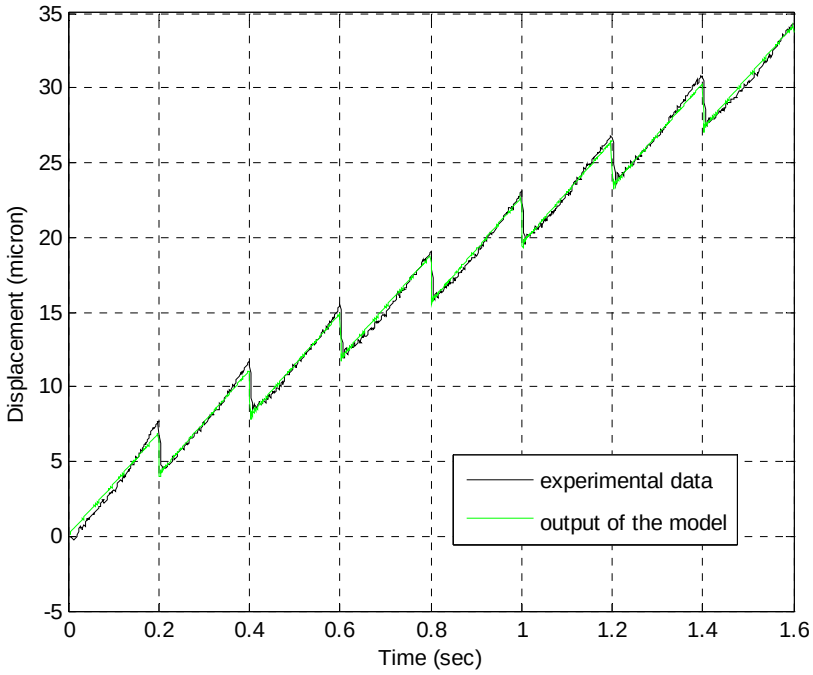

Figure 5.2 Experimental Data and Output of the Model, as the Sawtooth Voltage with a Magnitude of 65 volts and a Frequency of 5 Hz Applied to the PDSS actuator

The parameters to be estimated are σ_0, σ_1 and F_C, given in (3.18) and (3.23). Based on (3.18) to (3.22), a Simulink model of the PDSS actuator model was created, which is shown in Figure 5.3. The input to the PEA is the sawtooth wave. The combination of the PEA and the stage is represented by using a second order dynamic system with the parameters determined previously. The output of the PEA y, is the displacement of the stage, which is one of the inputs to the

friction model. The other input to the friction model, x_e, is the displacement of the end-effecter, which is the output of the PDSS actuator model. The difference between y and x_e, i.e., the relative displacement between the stage and the end-effecter, is then used by the friction subsystem. The details of this Simulink model of the PDSS actuator are given in Appendix 6. This model was applied to estimate the parameters σ_0, σ_1 and F_C in the friction model.

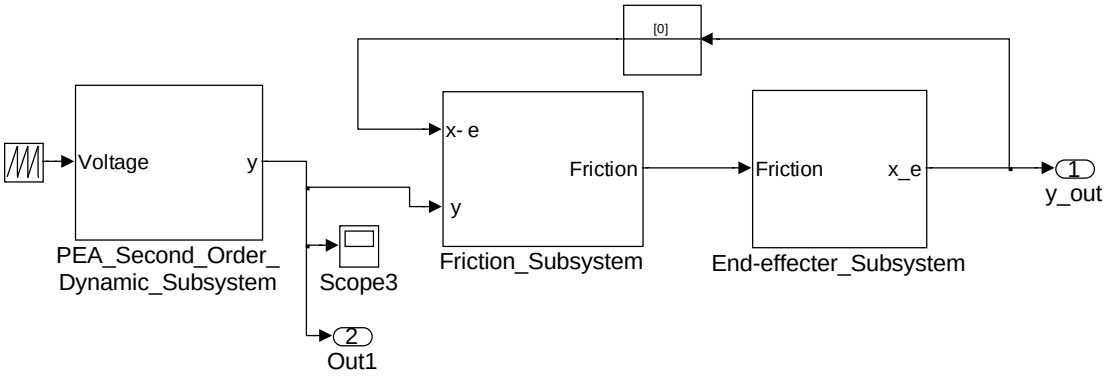

Figure 5.3 Simulink Model of the PDSS Actuator

On basis of the above Simulink model of the PDSS actuator, the parameters of the friction model were estimated by employing the function of "nlinfit" in Matlab. In detail, the first step of the estimation was to extract the useful data from the original experimental data. Specifically, some of the experimental data were cut off from the original data that were obtained as the sawtooth with magnitudes of 35, 55, 65, and 75 volts applied; and the program codes for this purpose is provided in Appendix 7. Also, the filtering technique was applied again in order to reduce the influence of noise involved in the recorded data. For this purpose, every three consecutive data were averaged. Once the data were prepared as described in the above, the function of "nlinfit"

was employed to estimate the parameters, and the program codes are provided in Appendix 8. This function estimates the parameters by starting with an initial guess and then altering the guess until the error or the difference between the measured displacements and the model predictions is converged becoming minimal. By doing so, the estimated values of the model parameters are σ_0 = 1399, σ_1 = 0.0349 and F_C = 0.5401. With the estimated parameters, the simulated displacements by the developed model are also shown in Figure 5.2 in a light (green) line for comparison.

5.4 PDSS Actuator Model Verification

Three experiments were conducted by applying 35, 55, and 75 volts sawtooth to the actuator to verify the effectiveness of the developed model. Figure 5.4 shows the measured displacements and the simulated ones from the developed model with the parameters identified in the preceding section. The coefficient of determination r^2 was calculate as 0.9979 for the 65 volts data, which was employed to the parameter estimation; and they are 0.9913 and 0.9985, respectively, for 55 and 75 volts data employed to the model verification. A good agreement is seen between the measured displacements and model predictions, indicating that the model developed in this study is promising for the end-effector displacement of the piezoelectric-driven stick-slip actuator.

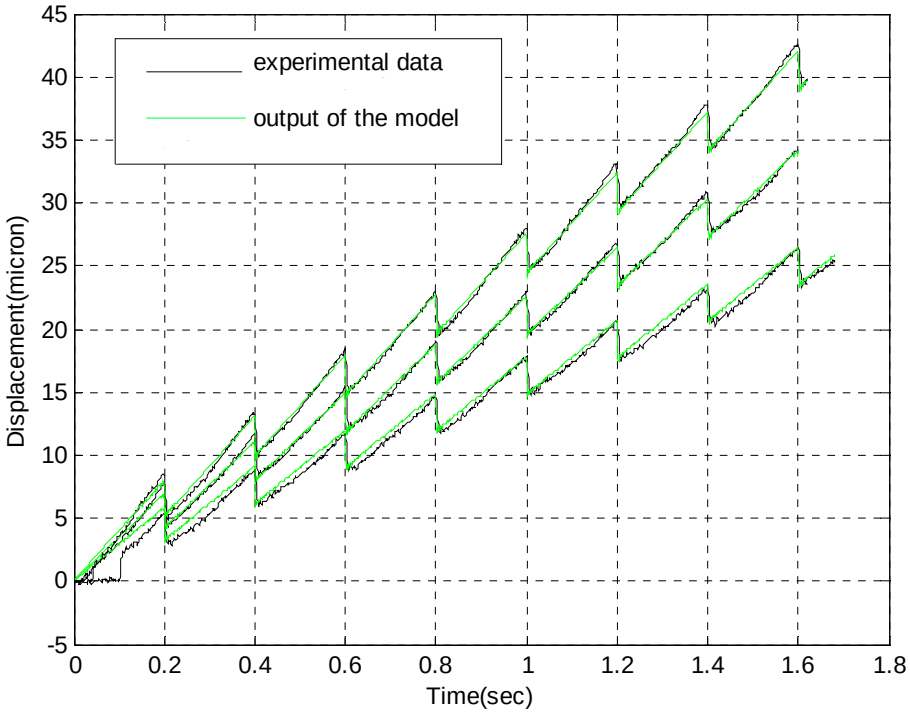

Figure 5.4 Experimental Data and Output of the Model, as the Sawtooth Voltage with Different Magnitudes and a Frequency of 5 Hz Applied to the PDSS Actuator

5.5 Summary

In this chapter, the identification of the parameters involved in the PDSS actuator model has been performed on the developed experimental system. This identification includes two steps: the first step is to estimate the parameters of the model of the combination of the PEA and the stage, and the second one is to determine the parameters of the friction model. Once the parameters are determined, the PDSS actuator model was examined by the experiments, as the different voltages were applied to the actuator. The results obtained from the experiments were compared to the simulation results, and it indicates the validity of the developed model.

CHAPTER 6 CONCLUSIONS AND FUTURE WORK

6.1 Summaries and Conclusions

In many applications of micropositioning and micromanipulation, the displacement range of an actuator is as vital as its precision. The PDSS actuator considered in this research is one of the solutions to, by utilizing the piezoelectric actuator (PEA) and the friction, produce displacements of a long range with a high resolution displacement. Representation of the dynamics of the displacement in such a PDSS actuator has proven to be challenging task due to the involvement of the PEA dynamics and the presliding friction; and the models for this purpose are lacking in the literature. This research is aimed to address this issue by developing a model for the PDSS actuator, in which both the PEA dynamics and the presliding friction and are addressed.

In the PDSS actuator, the PEA is used to drive a stage, so it is not a standalone device any more. Thus, its dynamics is different from the one where only a PEA is considered. In this research, the dynamics of the combination of a PEA and a stage with different masses was investigated and examined experimentally, and the results obtained suggests that this dynamics can be approximated by a second order dynamic system if the mass the stage is much greater than that of the PEA.

The modeling of presliding friction is of particular interest in this research due to the minute displacements concerned. The latest techniques for modeling enable us to represent the presliding friction. By reviewing and comparing four friction models, namely Dahl model, Reset Integrator model, LuGre model and Elastoplastic model, it is concluded that the LuGre model is the appropriate one for the friction in the PDSS actuator, due to its capability of taking into account the stiction, viscous friction and Stribeck effect simultaneously. This conclusion is also confirmed by both the simulations and the experiments.

On the basis of the aforementioned studies, a model for the PDSS actuator was developed to represent the dynamics of the displacement. The experiments were then carried out in order to identify parameters of this model and validate the developed model. These experiments were conducted on the PDSS actuator which was prototyped in this research. For the need in the experiment, a displacement measuring and data acquisition system was also developed based on dSPACE and Simulink. The parameters were identified by using two experiments, one experiment for the determination of the parameters of the second order system and other one for the determination of the parameters of the friction model. The identified parameters were then employed in the PDSS model to simulate the displacements and the results obtained were compared with the experimental results under the same operating conditions as the simulation. The comparison suggests that the model developed in this study is promising to represent the displacement of the PDSS actuator.

6.2 Future Work

While the PDSS actuator model developed in this study shows promising features, there are still some issues needed to be addressed, which could be the work pursued in the future research. One of the pieces of the work could be the use of the contact surfaces with different microstructures from the one used in this study in the PDSS actuator. This will enable the investigation into the influence of the contact surface on the actuator performance, thereby optimizing the actuator design.

Another piece of the future work could be implementation of various control strategies to the PDSS actuator for improved performance. The PDSS actuator prototyped in this research is simply an open loop system. Although its performance was stable and the experiments show a good repeatability, there is definitely a space for improvement. In addition, the nonlinearity of the PEA was not considered in this research, and also the oscillation of the displacement was observed in the experiments of using saw-tooth input signals. These issues could be addressed by applying control methods on the PDSS actuator.

The last piece of work suggested for the future could be the improvement of the displacement measuring and data acquisition system. While it works for the need of the present research, it accuracy could be a limited factor to future studies on the PDSS actuator. In the present research, it was observed that, if the displacement is too small, the noise overwhelms the measured displacement. As a result, small voltage couldn’t be applied to the PDSS actuator for experiments. In the present study, a few attempts were used to reduce the noise, which include

reducing the oscillation of the support frame of the PDSS actuator, insulating the measuring system from the possible electromagnetic disturbing, and employing filters in measuring system. It is suggested that more accurate displacement sensors, such as interferometers, could be used in the displacement measuring and data acquisition system for the future studies on the PDSS actuator.

LIST OF REFERENCES

[1] AEDL lab manual, "Experimental Setup"

[2] A.BERGANDER, J.-M.BREGUET and R.CLAVEL, "Micropositioners for microscopy applications and microbiology based on piezoelectric actuators", *Journal of Micromechanics*, Vol.2, No.1, pp.65-76 (2003)

[3] Benjamin Edinger, Mary Frecker, John Gardner, "Dynamic Modeling of an Innovative Piezoelectric Actuator for Minimally Invasive Surgery", *Journal of Intelligent Material System and Structures*, Vol. 11 October 2000

[4] Christine Meyer, Omar Sqalli, Heribert Lorenz, Khaled Karrai, "Slip-stick Step-scanner for Scanning Probe Microscopy", *Review of Scientific Instruments*, 76, 063706 2005

[5] Christopher Niezrecki, Diann Brei, Sivakumar Balakrishnan, and Andrew Moskalik, "Pieoelectric Actuation: State of the Art", The Shock and Vibration Design, Vol. 33, No. 4, 269-280, July 2001

[6] Ch. Renner, Ph. Niedermann, A. D. Kent, and *Φ*. Fischer, "A vertical piezoelectric inertial slider," *Review of Scientific Instruments*, vol. 61, pp. 965-967, 1990

[7] C. Niezrecki, D. Brei, S. Balakrishnan, and A. Moskalik, "Piezoelectric actuation: state of the art," *The Shock and Vibration Digest*, vol. 33, pp. 269-280, 2001.

[8] C. Canudas de Wit, H. Olsson, K. J. Astrom, P. Lischinsky, "A New Model for Control of Systems with Friction", *IEEE TRANSACTIONS ON AUTOMATIC CONTROL, VOL.40, NO.3*, MARCH 1995

[9] dSPACE Digital Signal Processing and Control Engineering GmbH, "Control Desk Experiment Guide" For ControlDesk Version 12 September 1999

[10] dSPACE Digital Signal Processing and Control Engineering GmbH, "DS1102 DSP Controller Board Installation and Configuration Guide"

[11] dSPACE Digital Signal Processing and Control Engineering GmbH, "Floating-Point Controller Board - DS1102 Hardware Reference",

[12] D. A. Haessig, Jr., B. Friedland, "On the Modeling and Simulation of Friction", *Journal of Dynamic Systems, Measurement, and Control*, vol.113, September 1991

[13] D.W. Pohl, "Dynamic piezoelectric translation devices", Review of Scientific Instruments, Vol.58, No.1, January 1987

[14] Ernest Rabinowicz, "The Nature of the Static and Kinetic Coefficients of Friction", *Journal of Applied Physics*, *Vol. 22, No. 11*, 1951

[15] F. P. Bowden and D. Tabor, "Friction: An Introduction to Tribology", *ANCHOR PRESS / DOUBLEDAY*, 1973

[16] Han J. M. T. A. Adriaens, Willem L. de Koning, and Reinder Banning, "Modeling Piezoelectric Actuators", *IEEE/ASME TRANSACTIONS ON MECHATRONICS*, VOL. 5. NO.4. DECEMBER 2000

[17] HORST CZICHOS, "TRIBOLOGY: a system approach to the science and technology of friction, lubrication and wear", *ELSVIER SCIENTIFIC PUBLISHING COMPANY*, 1978

[18] H. Olsson, "Doctoral Dissertation: Control System with Friction", Department of Automatic Control of Lund Institute of Technology, April 1996

[19] H. Olsson, K. J. Astrom, C. Canudas de Wit, M. Gafvert, P. Lischinsky, "Friction Models and Friction Compensation", *European Journal of Control*, v4, n3, 1998, p176-95

[20] Kaman Instrumentation Cooperation, "Application Guidelines for Inductive Displacement Measuring Systems"

[21] Kaman Instrumentation Corporation, "SMU-9000 User Manual"

[22] Melles Griot Company, "Piezoelectric Drives", *www. mellesgriot.com /resourcelibrary*

[23] M. Goldfarb and N. Celanovic, "Modeling Piezoelectric Stack Actuators for Control of Micromanipulation", *IEEE CONTROL SYSTEMS MAGAZINE*, Vol. 17, Pages. 69-79, 1997

[24] M. S. Hoogeman, *et al*., "Design and performance of a programmable-temperature scanning tunneling microscope," *Review of Scientific Instruments*, vol. 69, pp. 2072-2080, 1998

[25] NEC / TOKIN, "Multilayer Piezoelectric Actuators Vol. 02"

[26] Physik Instrumente Co., Ltd. *Tutorial: Piezo-electrics in Positioning Contents* www.physikinstrumente.com/en/products/piezo_tutorial

[27] Pierre Dupont, Vincent Hayward, Brian Armstrong, and Friedhelm Altpeter, "Single State Elastoplastic Friction Models", *IEEE TRANSACTIONS ON AUTOMATIC CONTROL*, VOL. 47. NO. 5, MAY 2002

[28] P. E. Tenzer and R. B. Mrad, "A systematic procedure for the design of piezoelectric inchworm precision positioners," *IEEE Transactions on Mechatronics*, vol. 9, pp. 427-435, 2004

[29] P.-A.J. Bliman, "Mathematical Study of the Dahl's friction model", *European Journal of Mechanics, A/Solids*, Vol.11, No.6, 1992

[30] Standards Committee of the IEEE Ultrasonics, Ferroelectrics, and Frequency Control Society, *IEEE Standard on Piezoelectricity*, 1987

[31] S.H. Chang and S.S. Li, " A high resolution long travel friction-drive micropositioner with programmable step size", *Review of Scientific Instruments*, Vol.70, Number 6, June 1999

[32] The Institute of Electrical and Electronics Engineers, Inc, "An American National Standard IEEE Standard on Piezoelectricity", ANSI/IEEE STD 176-1987

[33] The MathWorks, Inc., "Real-Time Workshop-For Use with SIMULINK User's Guide Version 3"

[34] Y. Zhang, W. J. Zhang, J. Hesselbach, and H. Kerle, "Development of a two-degree-of-freedom piezoelectric rotary-linear actuator with high driving force and unlimited linear movement ", *Review of Scientific Instruments*, vol. 77, 035112, 2006

APPENDICES

Appendix 1 Table of Calibration

Table 4.2 Calibration of Kaman Inductive Displacement Sensor by Manufacturer

5th Order Polynomial: Maximum error about 6 microns

	a	b	c	average	a	b	c	average
0.000	0.010	-0.001	0.000	0.003	0.000	-0.001	0.000	0.000
0.100	1.411	1.339	1.332	1.361	0.104	0.100	0.099	0.101
0.200	2.921	2.829	2.814	2.855	0.203	0.197	0.196	0.199
0.300	4.405	4.322	4.297	4.341	0.305	0.299	0.297	0.300
0.400	5.739	5.682	5.646	5.689	0.406	0.401	0.398	0.402
0.500	6.878	6.815	6.807	6.833	0.504	0.499	0.498	0.500
0.600	7.801	7.750	7.753	7.768	0.603	0.597	0.597	0.599
0.700	8.543	8.508	8.515	8.522	0.703	0.697	0.698	0.700
0.800	9.139	9.114	9.123	9.125	0.804	0.799	0.801	0.801
0.900	9.615	9.602	9.610	9.609	0.903	0.900	0.902	0.902
1.000	10.000	9.999	10.002	10.000	0.999	0.999	0.999	0.999

3rd Order Polynomial: Maximum error about 15 microns

	a	b	c	average	a	b	c	average
0.000	0.010	-0.001	0.000	0.003	-0.005	-0.006	0.006	-0.006
0.100	1.411	1.339	1.332	1.361	0.112	0.107	0.107	0.109
0.200	2.921	2.829	2.814	2.855	0.210	0.204	0.204	0.206
0.300	4.405	4.322	4.297	4.341	0.299	0.294	0.293	0.295
0.400	5.739	5.682	5.646	5.689	0.394	0.389	0.386	0.390
0.500	6.878	6.815	6.807	6.833	0.498	0.492	0.491	0.494
0.600	7.801	7.750	7.753	7.768	0.606	0.600	0.600	0.602
0.700	8.543	8.508	8.515	8.522	0.713	0.708	0.709	0.710
0.800	9.139	9.114	9.123	9.125	0.813	0.809	0.810	0.811
0.900	9.615	9.602	9.610	9.609	0.904	0.901	0.903	0.903
1.000	10.000	9.999	10.002	10.000	0.985	0.985	0.985	0.985

3rd Order Polynomial:
y = 1.191E-03x3 - 1.185E-02x2 + 9.852E-02x - 6.374E-03
5th Order Polynomial:
y = 2.191E-05x5 - 4.259E-04x4 + 3.497E-03x3 - 1.297E-02x2 + 8.674E-02x - 4.920E-04

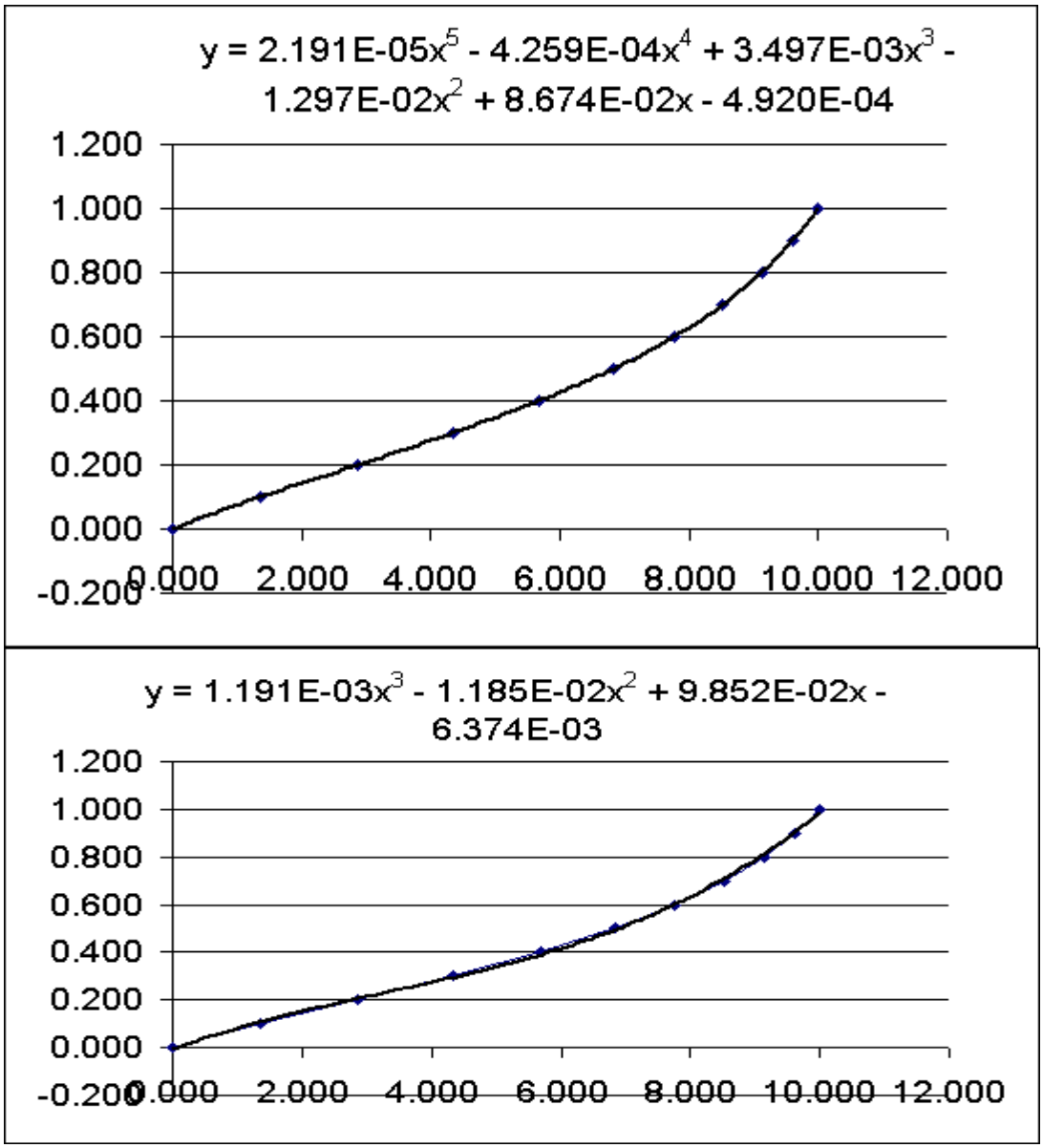
y = 2.191E-05x^5 - 4.259E-04x^4 + 3.497E-03x^3 - 1.297E-02x^2 + 8.674E-02x - 4.920E-04
1.200
1.000
0.800
0.600
0.400
0.200
0.000
-0.200
0.000
2.000
4.000
6.000
8.000
10.000
12.000
y = 1.191E-03x^3 - 1.185E-02x^2 + 9.852E-02x - 6.374E-03
1.200
1.000
0.800
0.600
0.400
0.200
0.000
-0.200
0.000
2.000
4.000
6.000
8.000
10.000
12.000

Appendix 2 Simulink Model of the PDSS Actuator Driven and Displacement Measuring in Sawtooth Wave Experiment

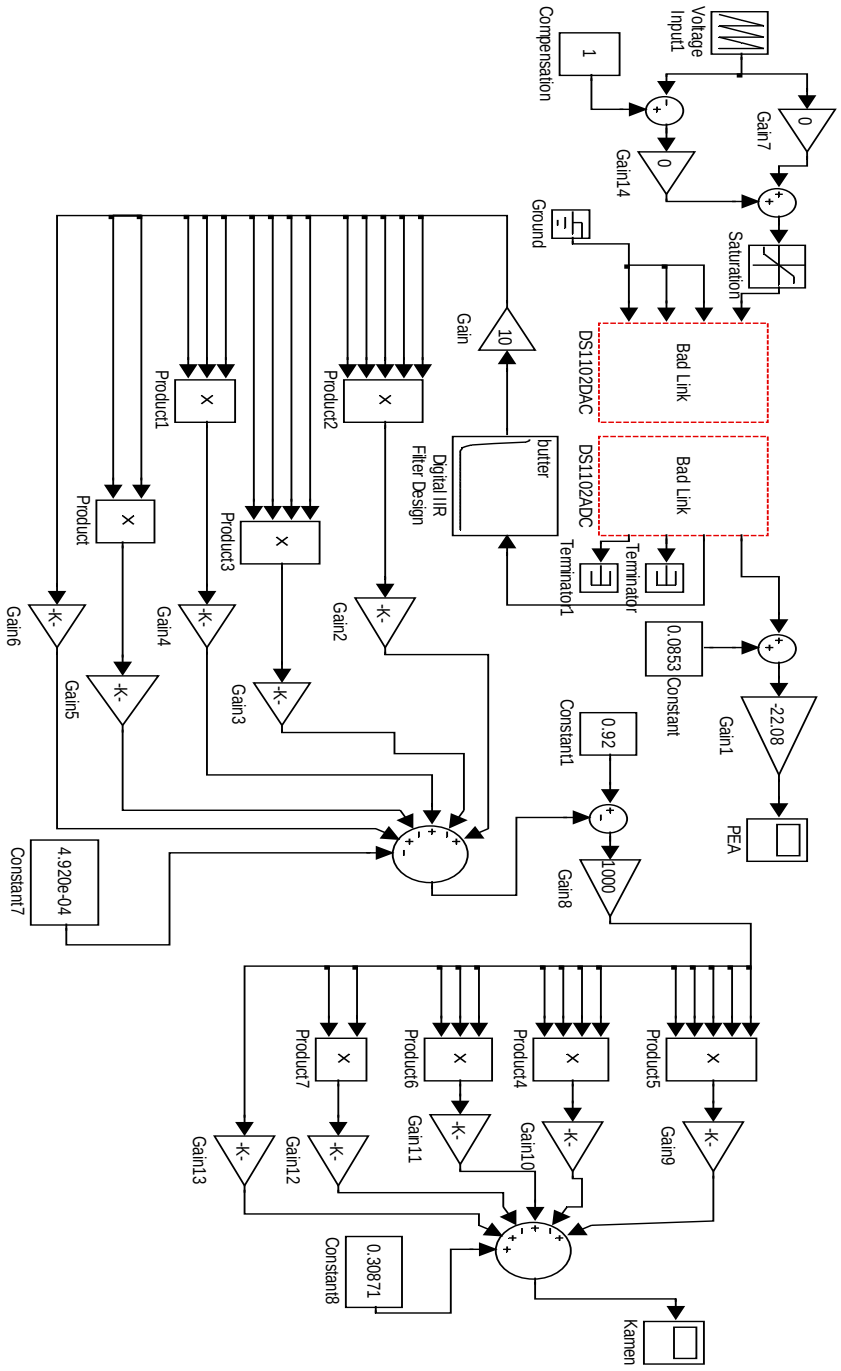

Appendix 3 Voltage Transforming Ration

Table 4.3 Voltage Transforming Ration between Input in Control Desk and the Exerted on PEA

Supposed PEA input (v)	0	3	5	10	15	20
dSPACE input (v)	0.00	0.0175	0.03	0.0615	0.0925	0.124
PEA input (v)	0.24	2.97	5.00	10.00	15.00	19.98
Supposed PEA input (v)	30	35	40	45	50	55
dSPACE input (v)	0.1865	0.218	0.2495	0.2805	0.312	0.343
PEA input (v)	29.96	35.04	40.02	45.02	50.03	55.03
Supposed PEA input (v)	60	65	70	75	80	
dSPACE input (v)	0.3745	0.4055	0.437	0.468	0.4995	
PEA input voltage(v)	60.01	65.01	70.00	74.99	79.97	

Appendix 4 Simulink Model of the PDSS Actuator Driven and Displacement Measuring in Step Response Experiment

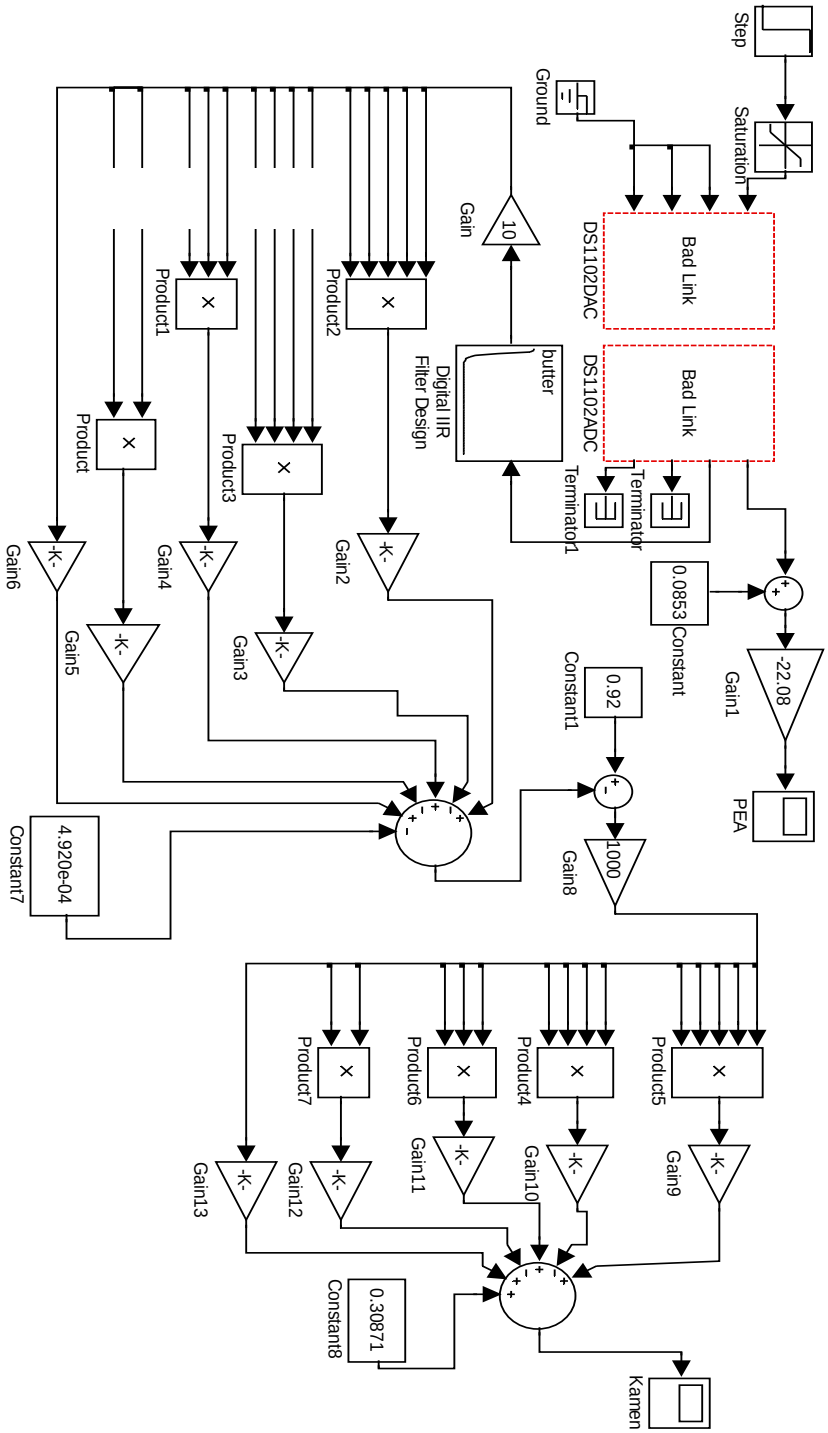

Appendix 5 Matlab Program for Second Order System Parameters Identification

```
% filename: Get_results_ready_step_response_with_a_block.m

% This program is to
% (1) load, select, and display the measured displeacements of the step
%     response of the pizeoelectric actuator with a block mass
connected,
% (2) identify the model parameters for the pizeoelectric actuator, and
% (3) display the model predictions and experimental results

clc, clear, clf;

% 1. load, select, and display the measured displeacements of the step
%    response of the pizeoelectric actuator with a block mass connected

     n = 100;            % Select n data for analysis
     k = 1;              % Select (k+1) data for average

     r = 4*20;           % Determine the starting point for the
evaluation
                         % of stead-state value, 20 points/ms
     rk = 20;            % Select (rk+1) data for average


   % 1.1 Load the data of 60 V and extract it
     load secpara_60v_1block_141206;  % Load measured data
     t = trace_x';                    % Time (s)
     Dis_e = trace_y(2,:)';           % Measured displacements (um)

     mm = 4000;                % Determine the cutting, i.e., t = 0.2 s
     m = mm + 16;              % Estimated delay = 16 / 20 (ms)
     Starting_time = t(m)


     sum = 0;                  % Calculate the bias before rising
     for i = (m-k):m
         sum = sum + Dis_e(i);
     end
     bias = sum/(k+1);

     sum = 0;                  % Calculate the stead-state value
     for i = (m+r):(m+r+rk)
         sum = sum + Dis_e(i);
     end
     ss (1) = sum/(rk+1)-bias;

     for i=1:n                       % show the extracted data curve
         t_cut(i) = t(m+i-1)-t(m);    % Relative time
```

```
        Dis_e_cut60(i) = Dis_e(m+i-1)-bias;
                                    % Relative value of displacemnt
    end
    plot(t_cut,Dis_e_cut60,'b-');
    hold on;

    [C_max(1), j] = max(Dis_e_cut60);  % Find the peak time and
magnitude
    T_p(1) = t_cut(j);

  % 1.2 Load the data of 70 V and extract it
    load secpara_70v_1block_141206;  % Load measured data
    t = trace_x';                    % Time (s)
    Dis_e = trace_y(2,:)';           % Measured displacements (um)

    sum = 0;                         % Calculate the bias
    for i = (m-k):m
        sum = sum + Dis_e(i);
    end
    bias = sum/(k+1);

    sum = 0;                         % Calculate the stead-state value
    for i = (m+r):(m+r+rk)
        sum = sum + Dis_e(i);
    end
    ss (2) = sum/(rk+1)-bias;

    for i=1:n
        t_cut(i) = t(m+i-1)-t(m);    % Relative time
        Dis_e_cut70(i) = Dis_e(m+i-1)-bias;
                                    % Relative value of displacemnt
    end
    plot(t_cut,Dis_e_cut70,'g-');
    hold on;

    [C_max(2), j] = max(Dis_e_cut70);
    T_p(2) = t_cut(j);

  % 1.3 Load the data of 80 V and extract it
    load secpara_80v_1block_141206;  % Load measured data
    t = trace_x';                    % Time (s)
    Dis_e = trace_y(2,:)';           % Measured displacements (um)

    sum = 0;                         % Calculate the bias
    for i = (m-k):m
        sum = sum + Dis_e(i);
    end
    bias = sum/(k+1);

    sum = 0;                         % Calculate the stead-state value
    for i = (m+r):(m+r+rk)
```

```
        sum = sum + Dis_e(i);
    end
    ss (3) = sum/(rk+1)-bias;

    for i=1:n
        t_cut(i) = t(m+i-1)-t(m);    % Relative time
        Dis_e_cut80(i) = Dis_e(m+i-1)-bias;
                                     % Relative value of displacemnt
    end
    plot(t_cut,Dis_e_cut80,'r-');
    hold on

    [C_max(3), j] = max(Dis_e_cut80);
    T_p(3) = t_cut(j);

    title('Step Response, with 1 Block ');  % Plot the 3 curves
    grid on;
    axis([0 0.005 0 12]);
    xlabel('Time (s)'), ylabel('Displacement (10^-3 mm)');

% 2. Identify the model parameters for the pizeo-actuator with mass.

    T_p_ave = mean (T_p);
    OP = (C_max - ss)./ss;           % Figure out average Overshoot
    OP_ave = mean (OP);

    damping_r = -log(OP_ave)/sqrt(pi^2+(log(OP_ave))^2)% Damping ratio
    natural_f = pi/(T_p_ave*sqrt(1-damping_r^2))       % Natural
frequence

% 3. Display the model predictions and experimental results
     num =  [natural_f^2];
     den = [1 2*damping_r*natural_f natural_f^2];

     PEA_tf = tf(num, den);


         sumrsqu = 0;                    % make a ram for calculating
r2

     for i = 1:3                     % Draw three simulated curve on
                                     % experiment results
         [Y,T] = step(PEA_tf, 0.005);
         plot(T, ss(i)*Y,'k-.');
         hold on
         yFit = ss(i)*Y
         nm = numel(yFit)
         yFit = yFit(1 : nm - 1)'    % select first 100 out of 101
data
                                     % for calculation of r2
```

```
        if i == 1
           Dis_cut = Dis_e_cut60(1 : nm - 1)
        elseif i == 2
           Dis_cut = Dis_e_cut70(1 : nm - 1)
        else
           Dis_cut = Dis_e_cut80(1 : nm - 1)
        end

         rsqu = cod(Dis_cut, yFit)
         sumrsqu = sumrsqu + rsqu

         aversqu = sumrsqu ./ i
      end


      Gain_D_V = mean(ss./[60 70 80])

% &. This section is restoring the comeout for future analysis
      save('expe_PZT_Stage_1block','Starting_time','damping_r',...
          'natural_f','Gain_D_V')
   % The End
```

Appendix 6 Matlab Program of the Calculation of Coefficient of Determination

```
%Filename: cod.m
%Instruction: This function works with
%             nlinfit_PZT_Friction_damper_3var.m   and
%             Get_results_ready_step_response_with_a_block.m

%             calculating the coefficient of determination of the
predict'
%             displacement after regression.
% --------

function rsqu = cod(Dis_cut,yFit)

yavg = sum(Dis_cut)./ numel(Dis_cut) % average of Dis_cut
sst = sum((Dis_cut - yavg).^2)       % calculate sst
sse = sum((Dis_cut - yFit).^2)       % calculate sse
rsqu = (sst - sse)./ sst   %Calculate the coefficient of determination

% end
```

Appendix 7 Simulink Model of PDSS Actuator

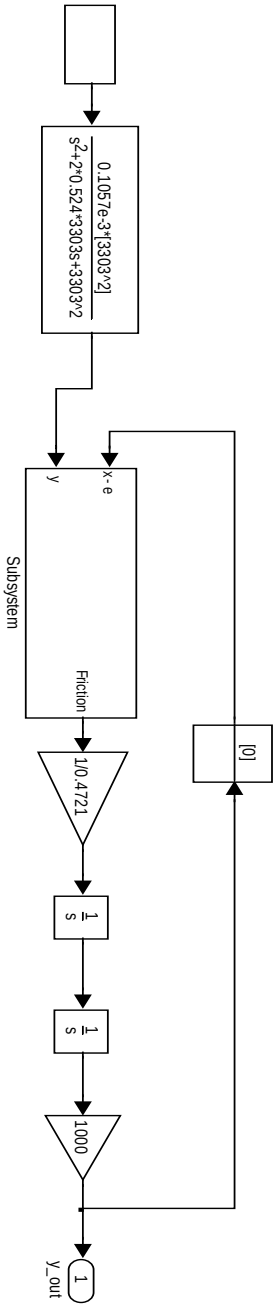

File name: nlinfit_PZT_Friction_damper.m

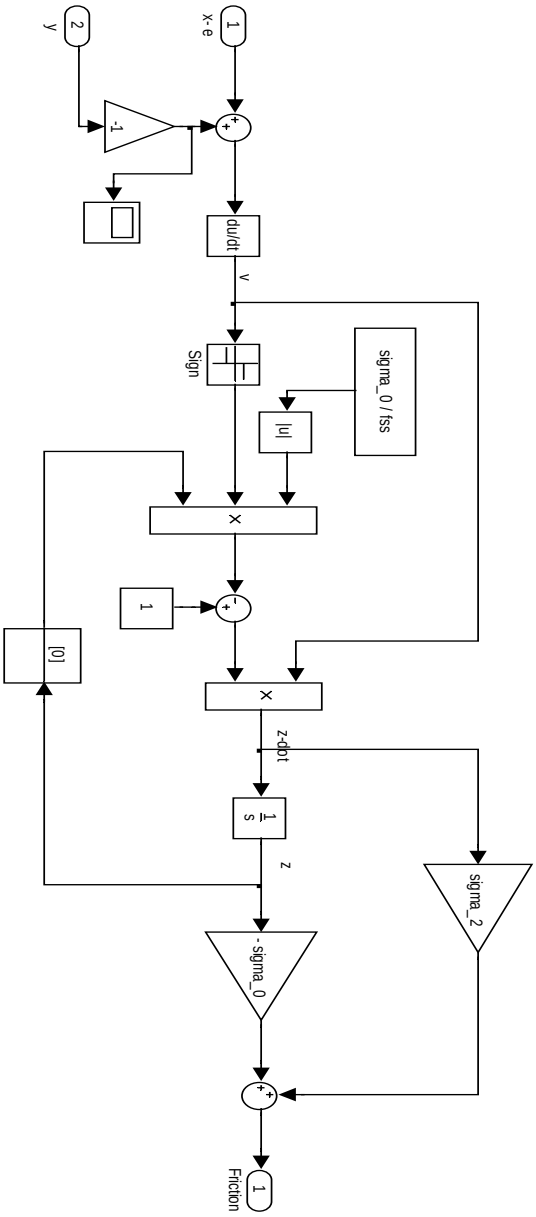

Friction Model of Simulink Model of PDSS Actuator (Subsystem of Above System)

Appendix 8 Matlab Program of the Experimental Data Manipulation for the Parameter Identification of the Friction Model of the PDSS Actuator with 20 Hz Sawtooth Input

```
% Fileanme: Experiment_results_extraction_20Hz.m
function [t_cut,Dis_cut] = Experiment_results_extraction_20Hz(freq,Peak_num)

% Instruction: This program is to extract the features from the measured
%              displeacemence for using in model identificaiton.

clc, clear;
     freq = 20;                  % frequency (Hz)
     Peak_num = 8;               % Seclect 8 peaks for analysis
     k = 20;                     % Select k data for average

     Ped_s = 1/freq;             % Time period (s)
     Ped_ms = 1000*Ped_s;        % Time period (ms)

% (1) Load the files of measurements with 20 Hz
%    Loading measured data

global volt;

if volt == 35;
     load saw_35v20hz_141206_2;
elseif volt == 55;
     load saw_55v20hz_141206_2;
elseif volt == 65;
     load saw_65v20hz_141206_2;
elseif volt == 75;
     load saw_75v20hz_141206_2;
     trace_y(2,:) = trace_y(3,:);  % for 75v the data of displacement is
                                   % in third row
end

     t = trace_x';                 % Time (s)
     Dis_e = trace_y(2,:)';        % Measured displacements (um)
     pn_ms = 1000*t(end)/(length(t)-1)     % Sampling time period (ms)
     d = length(t);
     n = Peak_num*Ped_ms/pn_ms + 780;      % Select n data for analysis
                                           % 780 may changes

% (2) Filtering and display the selected data

     for i=1:n
          t_n(i) = t(i);
          if i == 1
              FD(i) = Dis_e(1);
          elseif i == n
              FD(i) = Dis_e(n);
          else
              mid = (Dis_e(i-1)+Dis_e(i)+Dis_e(i+1));
              FD(i)=(mid)/3;
          end
     end
```

```
    plot(t_n,FD,'g-');
    grid on;
    xlabel('Time (s)'), ylabel('Displacement (10^-3 mm)');

% (3) Find the points with the max and peak displacements

    for i = Peak_num: -1:1
         if i == Peak_num       % Find the point with the max displacement
             [Dmax(i), Pmax(i)] = max(FD);
             Pmax(Peak_num) = Pmax(Peak_num)+6;   % Make some correction
          else         % Find the other points with the peak displacements
             Pmax(i) = Pmax(i+1) - round(Ped_ms/pn_ms);
             Dmax(i) = FD(Pmax(i));
         end
    end

    P0 = Pmax(Peak_num) - round(Peak_num*Ped_ms/pn_ms);
                               % Find the starting point
    D0 = FD(P0);               % P0 is position at the starting point
                               % D0 is displacement at the starting point

% (4) Calculate the bias displacement minus initial value
    sum = 0;
    for i = (P0-k+1):P0
        sum = sum + FD(i);
    end
    bias = sum/(k);

% (5) Find the values of a and b (a is the up-step and b is the down-step)
%                   a - b = c1
%                   Peak_num*a-(Peak_num-1)b = c2

    Dmax = Dmax - bias;
    for i=1:Peak_num
        if i==1
            sum = 0;
        else
            sum = sum + Dmax(i)-Dmax(i-1);
        end
     end
     c1 = sum/(Peak_num-1);

     c2 = Dmax(Peak_num);
     A = [1 -1;Peak_num -(Peak_num-1)];
     B = [c1;c2];
     x = A\B;
     a = x(1)
     b = x(2)

% (6) Display the adjusted data
      for i=1:(n-P0)
          t_cut(i) = t(P0+i-1)-t(P0);    % Relative time
          Dis_cut(i) = FD(P0+i-1)-bias;
                                     % Relative value of displacemnt
     end
```

```
     hold on;
     plot(t_cut,Dis_cut,'k-');

% (7) Display the sim curve with a and b
     slope = a/Ped_s;
     st = 0.001;
     t_sim = [0:st:(Peak_num*Ped_s)];
     for i=1:length(t_sim)
         if i == 1
            fl = 0;
            Dis_sim(i) = 0;
         elseif fl >= Ped_s
            fl = fl-Ped_s;
            Dis_sim(i) = Dis_sim(i-1) - b;
         else
            Dis_sim(i) = Dis_sim(i-1) + slope*st;
         end
         fl = fl+st;
     end

     hold on;
     plot(t_sim,Dis_sim,'r-');

     save Feat_75v20hz a b t_cut Dis_cut;

% (8) Load and display the above saved file
     pause(2);
     clf; clear;
     load Feat_75v20hz a b t_cut Dis_cut;
     plot(t_cut,Dis_cut,'k-');
     grid on;
     xlabel('Time (s)'), ylabel('Displacement (10^-3 mm)');

% The end
```

Appendix 9 Matlab Program of the Experimental Data Manipulation for the Parameter Identification of the Friction Model of the PDSS Actuator with 5 Hz Sawtooth Input

```
% fileanme: Experiment_results_extraction_5Hz.m
function [t_cut,Dis_cut] = Experiment_results_extraction_5Hz(freq,Peak_num)

% Instrcution: This program is to extract the features from the measured
%              displeacements for use in model parameters identificaiton.

clc, clear, clf;

global sigma_2;
global volt;
global Ped_s;
global sigma_0;
```

```
global fss;
global freq;

freq = 5;                    % frequency (Hz)
Peak_num = 8;                % Seclect 8 peaks for analysis
k = 20;                      % Select k data for average

Ped_s = 1/freq;              % Time period (s)
Ped_ms = 1000*Ped_s;         % Time period (ms)

% (1) Load the files of measurements with 5 Hz
if volt == 55,
      load saw_55v5hz_141206_2;
elseif volt == 35,
      load saw_35v5hz_141206_1;
elseif volt == 65,
      load saw_65v5hz_141206_1;
elseif volt == 75,
      load saw_75v5hz_141206_1;
end
     t = trace_x';                          % Time (s)
     Dis_e = trace_y(3,:)';                 % Measured displacements (um)
     pn_ms = 1000*t(end)/(length(t)-1);     % Sampling time period (ms)

     n = Peak_num*Ped_ms/pn_ms + 180;       % Select n data for analysis
                                            % 150 may changes

     for i=1:n                       % Filtering and display the selected data
          t_n(i) = t(i);
          if i == 1
              FD(i) = Dis_e(1);
          elseif i == n
              FD(i) = Dis_e(n);
          else
              mid = (Dis_e(i-1)+Dis_e(i)+Dis_e(i+1));
              FD(i)=(mid)/3;
          end
     end
    plot(t_n,FD,'g-');
    grid on;
    xlabel('Time (s)'), ylabel('Displacement (10^-3 mm)');

% (2) Find the points with the max and peak displacements
    for i = Peak_num: -1:1

         if i == Peak_num      % Find the point with the max displacement
             [Dmax(i), Pmax(i)] = max(FD);
          else          % Find the other points with the peak displacements
             Pmax(i) = Pmax(i+1) - round(Ped_ms/pn_ms);
             Dmax(i) = FD(Pmax(i));
         end
    end

    P0 = Pmax(Peak_num) - round(Peak_num*Ped_ms/pn_ms);
                              % Find the starting point
```

```
    D0 = FD(P0);              % Find the value of the starting point

% (3) Calculate the bias
    sum = 0;
    for i = (P0-k+1):P0
        sum = sum + FD(i);
    end
    bias = sum/(k);

% (4) Find the values of a and b (a is the up-step and b is the down-step)
%                   a - b = c1
%                   Peak_num*a-(Peak_num-1)b = c2

    Dmax = Dmax - bias;
    for i=1:Peak_num
        if i==1
            sum = 0;
        else
            sum = sum + Dmax(i)-Dmax(i-1);
        end
     end
     c1 = sum/(Peak_num-1);

     c2 = Dmax(Peak_num);
     A = [1 -1;Peak_num -(Peak_num-1)];
     B = [c1;c2];
     x = A\B;
     a = x(1)
     b = x(2)

% (5) Cut zero data off
     for i=1:(n-P0)
          t_cut(i) = t(P0+i-1)-t(P0);    % Relative time
          Dis_cut(i) = FD(P0+i-1)-bias;
                                         % Relative value of displacemnt
     end
     hold on;
     plot(t_cut,Dis_cut,'k-');

% (6) Plot the a b curve
     scope = a/Ped_s;
     st = 0.001;
     t_sim = [0:st:(Peak_num*Ped_s)];
     for i=1:length(t_sim)
         if i == 1
            fl = 0;
            Dis_sim(i) = 0;
         elseif fl >= Ped_s
            fl = fl-Ped_s;
            Dis_sim(i) = Dis_sim(i-1) - b;
         else
            Dis_sim(i) = Dis_sim(i-1) + scope*st;
         end
         fl = fl+st;
     end
```

```
    hold on;
    plot(t_sim,Dis_sim,'r-');

    save Feat_35v5hz a b t_cut Dis_cut;

    % Load and display the above saved fil
    pause(3);
    clf; clear;
    load Feat_35v5hz a b t_cut Dis_cut;
    plot(t_cut,Dis_cut,'k-');
    grid on;
    xlabel('Time (s)'), ylabel('Displacement (10^-3 mm)');

% The end
```

Appendix 10 Matlab Program for the Parameter Identification of the Friction Model of the PDSS Actuator

```
% Filename: nlinfit_PZT_Friction_damper_3var.m
% Instruction: This program is for employing nlinfit in sawtooth experiment
%              data regression by using 3 variables. The data for
%              regression is cut from the initial extracted data and total
%              7 waves.

clc,clear,clf;

global sigma_2;
global volt;
global Ped_s;
global sigma_0;
global fss;
global freq;
global pn_s;
global Dis_cut;


% 1. 20Hz sawtooth regression using nlinfit

% (1) Choose different frequency start simulation, there is slight time
%    Difference between experiment data and simulation, so a modification
%    was made.

freq = 20;                  % input frequency
%if freq == 20;
%else
peakt_n = 213;              % find the peakt_p(213) is 0.053 sec to compare
                            % to the simulation wave peak
period_n = 1512;            % determine cutting point at 1512 including 7
```

```
                          % waves
t_simpeak = 0.05;         % first peak time of simulationis 0.05 sec
Ped_s = 1/freq;           % the time period of an unit wave(s)
pn_s = 0.25e-3;           % sampling time period(s)

% (2) Using nlinfit find out parameters of friction model with 65v
%    experiment data, bring the parameters into 35v 55v 75v simulation,
%    then using "for" draw the curves four times.

i = 1;
for i = 1:4
    voltin = [35,55,65,75];   % define voltage input for 20Hz experi' data
    volt = voltin(i);         % choose the voltage one by one

% (3) Run Experiment_results_extraction_20Hz.m with different voltage input
%    and load the result.

Experiment_results_extraction_20Hz;   % Run the function in its name
load Feat_75v20hz.mat;                % Load result and get the variables
plot(t_cut,Dis_cut,'b-');
grid on;

% (4) Find out the bias of simula' model and cut experiment data of first
%     wave for more accurate regression.

T_err = t_cut(peakt_n) - t_simpeak;
                      % t_cut(peakt_n) is the time of the peakt_n, T_err is
                      % the time difference between Dis_cut first peak and
                      % the simu model first peak in seconds
n_t_err = round(T_err./pn_s);
                      % the number of data in T_err
t_cut = t_cut(n_t_err:period_n) - T_err;
                      % cut off again first 12 data of time on the head
                      % and cut off a group of data on the end
Dis_cut = Dis_cut(n_t_err:period_n);
                      % cut off again first 12 data of disp' on the head
                      % and cut off a group of data on the end
plot(t_cut,Dis_cut,'b-');
grid on;              % now the plot of data is shorter than previous one

% (5) Regression of 20Hz data with nlinfit

if volt == voltin(1),

sigma_in = [600, 0.03, 1.5];    % make initial values of model for nlinfit

[sigma_out,r,J] = nlinfit( t_cut,Dis_cut,@nlffuc_3var_single,sigma_in );
                           % applying sigma_in as the variable in nlinfit
sigma_20 = sigma_out       % show the value of sigma_out


% (6) plotting the regression figure

[yFit,delta] = nlpredci('nlffuc_3var_single',t_cut,sigma_out,r,J);
```

```
plot(t_cut,Dis_cut,'k-',t_cut,yFit,'r-'),grid on;
hold on;

rsqu = cod(Dis_cut, yFit)       % calculate the coefficient of
                                % determination

time_1 = t_cut;           % save the t_cut; Dis_cut; yFit for plotting
Displa_1 = Dis_cut;
DFit_1 = yFit;

% (7) Using new sigma_0; sigma_2 simulating and plotting the predicted
%    curve with 35v, 55v, 75v input voltage, and plot the curves

elseif volt ~= voltin(1);

sigma_0 = sigma_20(1);        % put new regressed parameters for simulink
sigma_2 = sigma_20(2);        % model
fss = sigma_20(3);

[t_cut20,x,y20] = sim('PZT_Friction_damper.mdl',length(t_cut)*pn_s);


    leth = length(y20)- 1;
    h = 0;                    % prepare counter
    y = 0;                    % clear y as displacement recorder
for l = 1:10:leth;             % choose 1 out of 4 simulink data to get
                              % same size of array as experiment data
    h = h+1;
    t_cut(h) = t_cut20(l);
    y(h) = y20(l)';
end

yout = 1000*y;
plot(t_cut, Dis_cut,'k-',t_cut, yout,'r-'),grid on;
                               % plot the curves with regressed parameters
yFit = yout;
rsqu = cod(Dis_cut, yFit)       % calculate the coefficient of
                                % determination

% (8) Save the simulation results into new variables for plotting

if i == 2,
    time_2 = t_cut;
    Displa_2 = Dis_cut;
    DFit_2 = yout;

elseif i == 3,
    time_3 = t_cut;
    Displa_3 = Dis_cut;
    DFit_3 = yout;

elseif i == 4
    time_4 = t_cut;
```

```
    Displa_4 = Dis_cut;
    DFit_4 = yout;

end                             % end of this if circle
end                             % end of voltage choosing if circle

i = i+1;                        % finish one circle go to circulate again

end                             % end of for

% (9) Plot out the final regression disgram

plot(time_1,Displa_1,'k-',time_1,DFit_1,'g-','LineWidth',0.2); hold on;
plot(time_2,Displa_2,'k-',time_2,DFit_2,'g-','LineWidth',0.2); hold on;
plot(time_3,Displa_3,'k-',time_3,DFit_3,'g-','LineWidth',0.2); hold on;
plot(time_4,Displa_4,'k-',time_4,DFit_4,'g-','LineWidth',0.2); hold on;
grid on;
xlabel('Time(sec)'),ylabel('Displacement(micron)');
%axis([0 0.45 0 0.04]);
title('Sawtooth-output-20Hz')

%end                             % jump to 5 Hz regression directly

% 2. 5Hz sawtooth regression with nlinfit

% (1) Choose different frequency start simulation,

freq = 5;                   % input frequency
Ped_s = 1/freq;             % the time period of an unit wave(s)
pn_s = 1e-3;                % sampling time period(s)

% (2) Using nlinfit find out parameters of friction model with 35v
%    experiment data, bring the parameters into 35v 55v 75v simulation,
%    then using "for" draw the curves four times.

i = 1;
for i = 1:4
    voltin = [65,35,55,75];     % define voltage input for 5Hz
    volt = voltin(i);

% (3) Run Experiment_results_extraction_5Hz.m with different voltage input
%    and load the results.

Experiment_results_extraction_5Hz
load Feat_35v5hz

my_opts = statset('DerivStep',6.000e-008)

% (4) Regression of 5Hz data with nlinfit to determine parameters

if volt == voltin(1),

sigma_in = [1000, 0.03, 1.5];          % make initial values of model
```

```
[sigma_out,r,J] = nlinfit(
t_cut,Dis_cut,@nlffuc_3var_single,sigma_in,my_opts);
                                % applying sigma_in in nlinfit
sigma_5 = sigma_out             % show the value of sigma_out

% (5) plotting the regression figure

[yFit,delta] = nlpredci('nlffuc_3var_single',t_cut,sigma_out,r,J);

plot(t_cut,Dis_cut,'k-',t_cut,yFit,'g-'),grid on;
hold on;

rsqu = cod(Dis_cut, yFit)       % calculate the coefficient of
                                % determination


time_1 = t_cut;
Displa_1 = Dis_cut;
DFit_1 = yFit;

% (6) Using new sigma_0; sigma_2 simulating and plotting the predicted
%    curve with 35v, 55v, 75v input voltages

elseif volt ~= voltin(1);
sigma_0 = sigma_5(1);
sigma_2 = sigma_5(2);
fss = sigma_5(3);

[t_cut5,x,y5] = sim('PZT_Friction_damper.mdl',length(t_cut)*pn_s);
                                % simulaiton with t_cut time
    leth = length(y5)-4;        % cut off 4 data reducing length of
                                % compassed data by one
    h = 0; y = 0;
for l = 1:40:leth;               % choose 1 out of 4 simulink data to get
                                % same size of array as experiment data
    h = h+1;
    t_cut(h) = t_cut5(l);
    y(h) = y5(l)';
end

yout = 1000*y;
plot(t_cut, Dis_cut,'k-',t_cut, yout,'r-'),grid on;

yFit = yout;
rsqu = cod(Dis_cut, yFit)       % calculate the coefficient of
                                % determination

% (7) Save the simulation results into new variables for plotting

if i == 2,
    time_2 = t_cut;
    Displa_2 = Dis_cut;
    DFit_2 = yout;
```

```
elseif i == 3,
    time_3 = t_cut;
    Displa_3 = Dis_cut;
    DFit_3 = yout;

elseif i == 4
    time_4 = t_cut;
    Displa_4 = Dis_cut;
    DFit_4 = yout;

end                              % end of this if circle
end                              % end of voltage choosing if circle

i = i + 1;                       % finish one circle go to circulate again

end

% (8) Plot out the final 5Hz regression disgram

plot(time_1,Displa_1,'k-',time_1,DFit_1,'g-','LineWidth',0.2); hold on;
%plot(time_2,Displa_2,'k-',time_2,DFit_2,'g-','LineWidth',0.2); hold on;
plot(time_3,Displa_3,'k-',time_3,DFit_3,'g-','LineWidth',0.2); hold on;
plot(time_4,Displa_4,'k-',time_4,DFit_4,'g-','LineWidth',0.2); hold on;
grid on;
xlabel('Time(sec)'),ylabel('Displacement(micron)');
%axis([0 0.45 0 0.04]);
title('Sawtooth-output-5Hz')

% end
```

Appendix 11 Matlab Program of Nlinfit Function of PDSS Actuator Model

```
% Filename:  nlffuc_3var_single.m
function [yout] = nlffuc_3var_single(para,t_cut)
% Instruction: This program is function of nlinfit_PZT_Friction_damper_3var
%              _single.m for regression with nlinfit. This program invokes
%              the simulink model PZT_Fricton_damper.mdl as function to
%              reckon sigma_0, sigma_2 and fss with 5hz and 20hz.
%
%
global sigma_2;
global volt;
global Ped_s;
global sigma_0;
global fss;
global freq;
global pn_s;
global Dis_cut;
```

```
sigma_0 = para(1);
sigma_2 = para(2);
fss = para(3);

% 1. Running the model with 5 Hz and 20 Hz seperately, 5 Hz first

if freq == 5;                   % run with 5 Hz
    lth = length(t_cut);        % send length of t_cut to lth for later use
    [t_cut, x, y] = sim('PZT_Friction_damper.mdl',length(t_cut)*pn_s);
                                % now the t_cut has been changed
    leth = length(y) - 1;       % cut 20 off length of y equal to cut 1 off
                                % experiment data

    j = 0;
for i = 1:40:leth;              % choose 1 out of 4 simulink data to get
                                % same size of array as experiment data
    j = j+1;
    y5hz(j) = y(i)';
    t_cut5(j) = t_cut(i)';
end
    yout = 1000*y5hz;           % convert the data into micrometer
    sigma_0,
    sigma_2,
    fss,

plot(t_cut5,yout,'b-',t_cut5,Dis_cut,'k-');

% 2. Running the model with  20 Hz,

else

    [t_cut,x,y] = sim('PZT_Friction_damper.mdl',length(t_cut)*pn_s);
                                % time length used to fit the size of array
                                % of experiment data,
    leth = length(y) - 1;       % cut 5 off length of sim results y equal
                                % to cut 1 off length of experiment data
    j = 0;
for i = 1:10:leth;               % choose 1 out of 4 simulink data to get
                                % same size of array as experiment data
    j = j + 1;
    y20hz(j) = y(i)';
    t_cut20(j) = t_cut(i)';
end
    yout = 1000*y20hz;          % convert the data into micrometer
    sigma_0,
    sigma_2,
    fss,

plot(t_cut20,yout,'b-',t_cut20,Dis_cut,'k-');
end



% The end
```